
Article:
Yao, X., Cseh, L., Zeng, X. et al. (3 more authors) (2017) Body-centred cubic packing of spheres-the ultimate thermotropic assembly mode for highly divergent dendrons. Nanoscale Horizons, 2 (1). pp. 43-49. ISSN 2055-6756

https://doi.org/10.1039/c6nh00155f

Body-centred cubic packing of spheres – The ultimate thermotropic assembly mode for highly divergent dendrons

Xiaohong Yao[1], Liliana Cseh[1,2], Xiangbing Zeng[3], Min Xue[1], Yongsong Liu[1], Goran Ungar[1,3,*]

[1]Department of Physics, Zhejiang Sci-Tech University, Xiasha College Park, Hangzhou 310018, China
[2]Institute of Chemistry, Timisoara of Romanian Academy, Timisoara – 300223, Romania
[3]Department of Materials Science and Engineering, University of Sheffield, Sheffield S1 3JD, U.K.

Abstract

We have synthesised sodium tris(alkoxy)benzoates in which one of the three alkyl chains branches further into three $C_{18}H_{37}$ chains. These AB5 hyperbranched minidendrons melt directly into a body-centred cubic (BCC) mesophase formed by spherical "micelles". In contrast, their non-branched counterparts display various mesophases before they turn BCC on heating. This agrees with the predictions from a numerical geometric model that relates the shape of the molecular wedge to the type of mesophase they adopt. The spheres were found to shrink in volume on heating and expand on cooling, as molecules, in some cases nearly half of them, are ejected and again reintegrated in the spheres. The ejection of dendrons is caused by their lateral thermal expansion. The BCC appears to be the ultimate mesophase for the extremely divergent wedges such as the hyperbranched minidendrons. In dendrons with chains of unequal length, the sphere size is fixed by the shorter chains, the longer ones back-folding or interdigitating to effectively widen the wedge. The new understanding of their assembly will help design new dendrons, e.g. for better encapsulation of guest molecules.

Main text

Taper-shaped molecules that possess a degree of amphiphilicity often exhibit liquid crystal (LC) phases with 2-D or 3-D periodicity. The majority of such compounds so far have been dendrons and "minidendrons", typically containing an aromatic core and flexible terminal alkyl or oligo(ethylene oxide) chains.[1,2,3,4,5] Taper-shaped mesogens, including dendrons, are some of the most fundamental and widespread building blocks in supramolecular chemistry. They have been attached to moieties such as organic semiconductors,[6,7] ionic conductors,[8,9,10,11,12] crown ethers,[13,14] donor-acceptor complexes,[15,16] polymers,[17,18,19] peptides,[20] nanoparticles[21,22] etc. This way "dendronized" functional materials may be created that can be used in a variety of potential applications.[23] The most common supramolecular objects that such dendrons or dendronized compounds form are columns and spheres. When the tapered molecules are fan-shaped, i.e. when they can easily fit in a plane, the compound is likely to form a columnar phase. Oversimplified, the pizza-slice-like molecules self-assemble into disks ("pizzas") which, in turn, stack on top of each other and form columns which, finally, assemble on a 2-D lattice, usually hexagonal. However, if the peripheral chains have a cross-section larger than would fit in a plane, such tapered molecules adopt a conical shape. The cones then assemble into spheres which, in turn, pack on 3-D lattices.[24]

Fan shape induced columnar organization, often due to the attachment of alkoxyphenyl, or Percec-type dendrons,[1] can be usefully exploited in many ways, e.g. in forming 1-D electronic[6,7] and ionic[8,9,10,11,12] conductors, in encapsulating light-emitting polymers,[25] forming artificial ionic channels etc. Temperature-induced transition from columns to spheres can be

used e.g. to create a thermal switch, whereby an ionically or electronically conducting columnar molecular wire would split into isolated spherical fragments at a pre-set temperature and break the circuit.[26] Spherical assembly can also in principle be used to encapsulate and isolate molecules such as organic light emitters to prevent radiationless energy transfer. But this development has been hampered by high sensitivity of supramolecular thermotropic micelles to insertion of any larger entity at the thin end of the molecular wedge thereby effectively reducing the taper and reverting the spheres to columns. A better fundamental understanding of the spherical assembly of tapered molecules is keenly needed. There are also remarkably few theoretical or simulation studies on the subject.[27,28]

The lattices formed by the supramolecular spheres, or micelles, are the same as those found in metals and alloys, albeit on a length-scale an order of magnitude larger, with inter-sphere spacing typically of the order of 2-4 nm.[29] Wedge-shaped compounds have been found to exhibit the following micellar LC phases: the cubic phase with $Pm\bar{3}n$ symmetry and 8 spheres in a unit cell, known in metallurgy as A15;[30,31] the tetragonal $P4_2/mnm$ phase (the "σ-phase") with 30 spheres;[32] the body-centred cubic (BCC), space group $Im\bar{3}m$ and with only 2 spheres per cell;[17,33] and the aperiodic dodecagonal liquid quasicrystal (LQC).[34] Recently compiled statistics on the occurrence of these phases[24] based on the data in ref. 1 is summarized in Table 1. The $Pm\bar{3}n$ cubic phase is found to be by far the most common, observed in 84% of all appearances of micellar phases, and 55% of all LC phases detected in such compound, including columnar and smectic phases. On the other hand the simplest micellar phase, the BCC, is the least represented, showing up in only 2% of micellar cases.

Table 1. Occurrence (number of reported compounds) of different LC phases in Percec-type dendrons based on benzylether, phenylpropyl ether, biphenyl-4-methyl ether and biphenylpropyl ether of generations 2 and higher (compiled from information in 1).[a,b]

Configuration at root[c]	cubic (A15) ($Pm\bar{3}n$)	tetragonal (σ) ($P4_2/mnm$)	dodecagonal quasicrystal	BCC ($Im\bar{3}m$)
AB3	50 (94%)	0	2 (4%)	1 (2%)
AB2 ortho	42 (91%)	3 (7%)	1 (2%)	0
AB2 meta	7 (37%)	7 (37%)	4 (11%)	1 (3%)
total	99 (**84%**)	10 (**8%**)	7 (**6%**)	2 (**2%**)

[a] Percentages are relative to the total number of occurrences of micellar 3-D phases. [b] Phases occurring in the same compound at different temperatures are also counted. [c] Indicates substitution at the exterior side of the phenyl ring closest to the apex of the dendron: "AB3" = 3,4,5-, "AB2 ortho" = 3,4- and "AB2 meta" = 3,5-substitution.

Table 1 also points to some interesting correlations between molecular architecture and the phase type; e.g. there is large preference for the narrow apex ortho AB2 dendrons to form the $Pm\bar{3}n$ phase in contrast to the wider apex meta AB2 dendrons which show, if anything, a slight preference for the dodecagonal phase and its close approximant the σ-phase. In this communication we concentrate on the BCC phase. At first sight it is indeed surprising that this simple packing is the rarest. In fact, however, there is a group of compounds where the BCC is well represented, i.e. the 3,4,5-tris(alkoxy)benzoate salts of alkali metals or their sulfonate equivalents, as well as some other such AB3 "minidendrons", including those attached to a

polymer backbone.[17,35,36,37,38] These can be regarded as 1st generation dendrons; when the alkyl chains are dodecyl or longer, they all display LC phases of which the BCC occurs at the highest temperatures. All of these salts also form other stable LC phases at lower temperatures. In order to understand this behaviour we first discuss a semiquantitative geometric model that relates molecular shape with the packing mode of the spherical micelles. Since the model predicts that increased branching should stabilize the BCC, we decided to test our model by synthesising new "hyperbranched" alkoxybenzoate salts and test our model's predictions. From the practical viewpoint, if we want to encapsulate guest species into the micelles, thereby inevitably reducing the effective taper angle, we need to start with a wedge as highly tapered as possible in the first place. The second objective is to explore what happens when the terminal chains are not all of the same length, as they have been in most if not all of the previously reported studies.

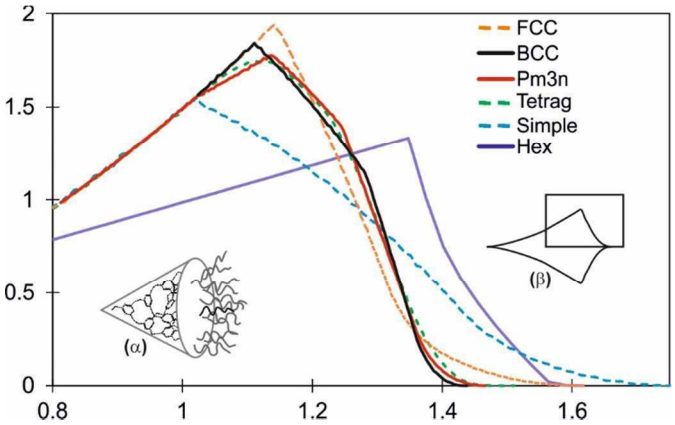

Figure 1 Radial distribution of volume functions *dV/dr* for different micellar phases: face-centred cubic (FCC), BCC, $Pm\bar{3}n$, $P4_2/mnm$ (Tetrag) and simple cubic, as well as for the hexagonal columnar phase (Hex, Col_h). The curves have been normalized to the same total volume of a micelle (disk in the case of Col_h). Abscissa scale is in arbitrary units. For explanation of insets see text (*cf* refs. 32 and 39).

In order to explain why spherical supramolecular dendrimers pack on different lattices, the average radial distribution functions of volume *dV*/*dr* have been calculated for different 3-D lattices with spherical motifs.[32, 39] These functions give the ideal shapes of wedge-shaped molecules that would fill the unit cell of a given phase perfectly uniformly. The spheres of radius *r* are allowed to grow simultaneously from their centres. Let $v_i(r)$ be that part of sphere *i* which does not overlap with another sphere. The graphs in Figure 1 show the averaged functions *dV*/*dr*, where $V = (1/N)\sum_{i=1}^{N} v_i$ is the mean volume *v*, and *N* is the number of spheres in the unit cell. Before the spheres impinge on one another, all curves are parabolae, since the surface of a sphere is $A(r)$ = d*v*/d*r* $\propto r^2$. But once they clash, the ascent of d*v*/d*r* either slows down ($Pm\bar{3}n$, tetragonal) or starts to drop (BCC, FCC, simple cubic). Eventually *dV/dr* goes to zero when all space is filled. The shape of *dV/dr* beyond the first clash is different for different lattices. In Figure 1 we also show the *dV/dr* curve for the hexagonal columnar (Col_h) phase. Here the cylinders rather than spheres grow from their central axis; thus *dV/dr* is linear with *r* before the cylinders clash.

A way to relate the *dV*/*dr* functions to the molecular shape is to imagine the conical molecule (inset α in Figure 1) rolled out flat into a parabolic (r^2) fan as schematically drawn in inset β in Figure 1. The ideal envelope of the molecular fan for each phase is represented by

the corresponding *dV*/*dr*, with *r* = 0 at the acute apex of the molecule. The rectangle in inset β indicates the limited region of *dV*/*dr* shown in the diagram.

The *dV*/*dr* distribution for BCC differs from those for $Pm\bar{3}n$ and *P*4$_2$/*mnm* in that it has a slightly higher peak and shorter tail. This change in molecular envelope is expected to occur at increasing temperatures due to lateral thermal expansion of the flexible chains requiring a higher *dV*/*dr* peak, and longitudinal contraction of the chains requiring a shorter *dV*/*dr* tail. The *dV/dr* curves for $Pm\bar{3}n$ and *P*4$_2$/*mnm* phases are similar to each other, and indeed the two phases have often been found to appear interchangeably.

A brief comment on the FCC phase, whose *dV/dr* is identical to that of the other "close packed" structure, the hexagonal close packing (HCP). Neither have yet been reported in thermotropic tapered compounds. The likely reason is the presence of large octahedral in addition to the small tetrahedral interstices. To reach the centres of the former, a long stretched chain is needed - see the long tail of the *dVdr* curve for FCC. One can speculate that to form the FCC or HCP phase the dendron would have to have perhaps one of the chains very long to match the long tail of the *dV/dr*. Possibly it may also need one or two short branches in addition to comply with the high peak of the FCC curve.

The divergence of the wedge-shaped molecule can be approximated in general by *dV/dr* = kr^p. A rough guide to phase type that such wedge-shaped molecules would form is given as follows.[24] $p \approx 0$: smectic; $0 < p < 1$: bicontinuous cubic; $p \approx 1$: columnar; $p \approx 2$: micellar (cubic or other symmetries). Figure 1 suggests that, as a crude approximation, the value of *p* also plays a part in determining which of the micellar phases is likely to be adopted by the compound, a higher *p* favouring the BCC and a lower *p* favouring the $Pm\bar{3}n$ phase.

Here we explore the high end of *p* and try to make the wedge more "exponential", i.e. make its width increase more steeply at larger *r*. Sodium salts **12^{2}18^{3}Na** and **18^{5}Na** were thus synthesised, each having one of their three alkoxy chains carrying a further three-way branching point based on pentaerythritol. A small branching group is used instead of the usual bulkier phenyl group to keep the wedge narrow near the root (small *r*), and thus increase the divergence *p*. The asymmetric compound **12^{2}18^{3}Na** has the branched chain at the 3-position, and the symmetric compound **18^{5}Na** at the 4-position. Furthermore, while in **18^{5}Na** the five chains are similar in length, in **12^{2}18^{3}Na** they differ in length considerably. These compounds were obtained by Williamson ether synthesis and the tris(alkyloxy)pentaerythritol intermediate was attached to the aromatic group by Mitsunobu reaction. The synthesis is given in Supporting Information (SI). For comparison the AB3 Na salts **12^{3}Na and 18^{3}Na**, with three unbranched $C_{12}H_{25}$ and $C_{18}H_{37}$ chains, respectively, have also been prepared; their synthesis has been described previously.[36] Table 2 gives the phase sequence of the compounds on first heating, as obtained from DSC and X-ray diffraction.

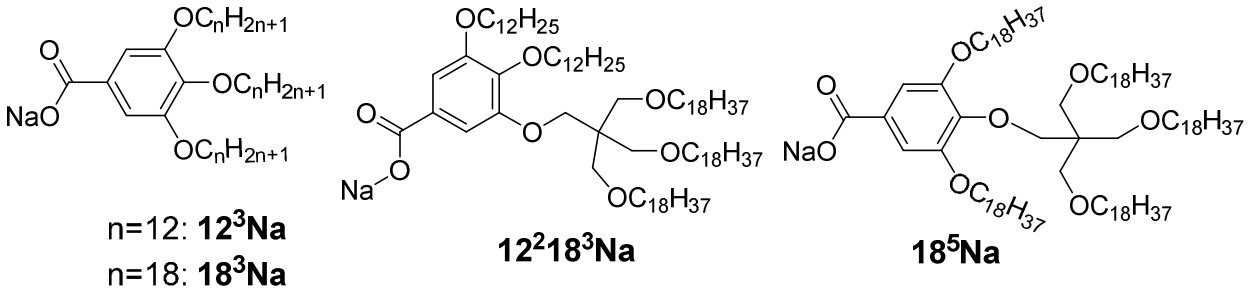

Table 2. Phases sequence and transition temperatures of the compounds studied*

Compound	Phases and transition temperatures (°C)
12^3Na	k 70 Col_r 91 Col_h 110 $Pm\bar{3}n$ 220 BCC decomp.
18^3Na	k 84 Col_h 104 BCC decomp
$12^2 18^3$Na	k 39 BCC 200 Iso
18^5Na	k 55 BCC decomp (>270)

*) k = crystal, Col_r = rectangular columnar, Col_h = hexagonal columnar, $Pm\bar{3}n$ and BCC = cubic, iso = isotropic liquid.

Figure 2 shows small-angle X-ray diffraction (SAXD) curves of the mesophases as a function of temperature, recorded during heating of compounds **12^3Na** and **18^5Na**. Equivalent SAXD scans for the other compounds are shown in SI (Figure S2). All compounds show 2D or 3D liquid crystal phases above the crystal melting point. In accordance with previous studies of tris(alkoxy)benzoates,[36] **12^3Na** and **18^3Na** start with the Col_h phase and end up in the BCC (space group $Im\bar{3}m$). In contrast, the hyperbranched compounds **$12^2 18^3$Na** and **18^5Na** melt directly into the BCC phase. Once having reached it, all compounds except **$12^2 18^3$Na** remain in the BCC phase until at least 270°C, where heating runs were interrupted for fear of decomposition. As an exception, **$12^2 18^3$Na** transforms to disordered isotropic liquid at 200°C, as is clear from Figure S2b. There is no detectable associated endotherm, meaning that the transition entropy is extremely low. In all cases the phase sequence is reversed on cooling. The diffraction intensities were used to reconstruct the electron density map of the BCC unit cell (Figure 3b), which clearly shows the spherical maxima at the corners and at the centre of the cell, marking the positions of the aromatic+ionic cores of the micelles. The low density continuum is uniformly filled with the alkyl chains, as indicated by the uniformly green colour in the map.

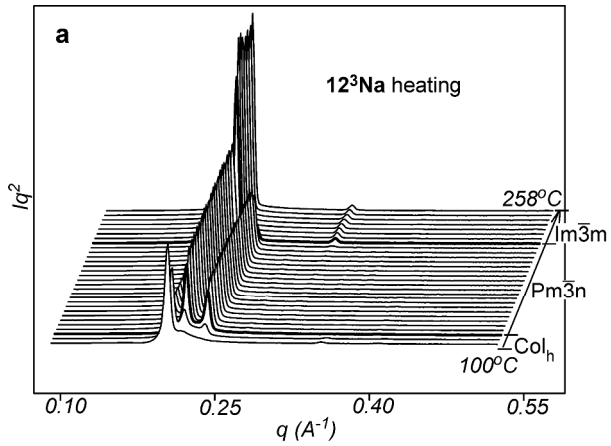

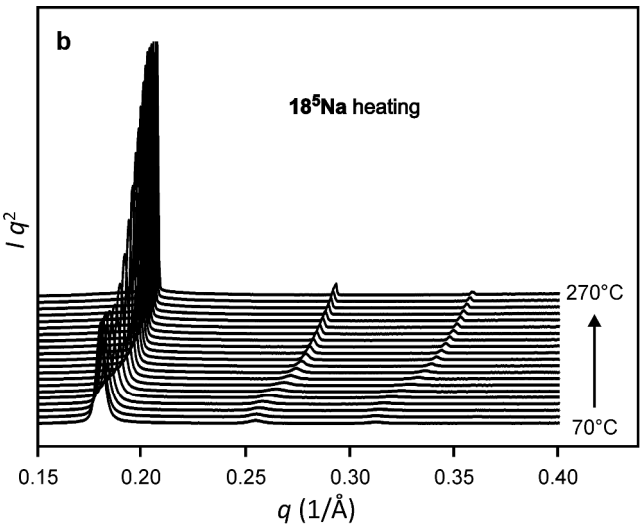

Figure 2. Series of SAXD curves (Lorentz-corrected) recorded during first heating (10 K min^{-1}) of solution-precipitated powder through the mesophase range. (a) **12^3Na**; (b) **18^5Na**. For clarity the shift between curves is tilted in (a) and vertical in (b). $q = 4\pi\ (\sin\theta)/\lambda$, where θ and λ are half scattering angle and wavelength.

The phase sequence Col_h → $Pm\bar{3}n$ → BCC with increasing *T* for **12^3Na** can be understood with reference to Figure 1, by noting the increasingly higher peak and shorter tail of the corresponding *dV/dr* curves. That is, the Col_h curve is suitable for linear wedges, such as found at lower temperatures in **12^3Na** and **18^3Na**, when their alkyl chains are mainly extended with few *gauche* conformers. At higher *T* and increasing *gauche* content, the chains expand laterally and contract longitudinally. A fan-cone transformation occurs in those two compounds, triggering the columnar – cubic phase transition. If the molecule was confined to a plane, this would be equivalent to a transition from linear to parabolic fan (see inset β in Figure 1), thus requiring the change to a phase structure with a parabolic rather than linear *dV/dr*. As the chain ends of **12^3Na** in the $Pm\bar{3}n$ phase continue to expand laterally on further heating, a *dV/dr* function with an even higher peak and shorter tail is required, and hence the $Pm\bar{3}n$ transforms to the BCC. In comparison, however, the longer chains of **18^3Na** require such additional lateral space already at lower *T*, which explains why this compound bypasses the $Pm\bar{3}n$ phase altogether.

Turning to the new hyperbranched salts, the fact that these only show the BCC phase is indeed what the *dV/dr* analysis predicts. Already at low *T* their wide aliphatic brushes require the *dV/dr* shape associated with the BCC phase. Their wide end is believed to be made even wider by the well-known preference for alkyl chain ends to adopt *gauche* conformations.[40] Hence these compounds indeed do not show any other LC phase but the BCC.

As temperature is increased, the BCC phase continues. It would appear that no other packing mode offers a better alternative for highly divergent molecules, i.e. a *dV/dr* with a higher peak and shorter tail. This would explain why BCC persists over a range of 200 K or more in most benzoate salts. However this does not prevent the dendrons from continuing to expand laterally and contract longitudinally with increasing *T*. Evidence can be found in the plots of BCC unit cell volume *vs. T* in Figure 3a. The cell volume, and hence the volume of the spheres, *decreases* on heating for all compounds studied, particularly steeply in **18^3Na** and **18^5Na;** in the latter case the micelle volume nearly halves in the measured *T* range. Our explanation of this remarkable behaviour is in that, as the solid angle Ω of the conical molecule expands, the

number of molecules $\mu = 4\pi/\Omega$, required to complete a sphere, decreases. Furthermore, longitudinal contraction of the chains also means that distant interstices can no longer be reached by the chain ends. Hence in order to fill space the lengthscale of the structure must contract. The thermal effect is equivalent to thermal shrinkage of rubber, an entropically driven phenomenon.[41]

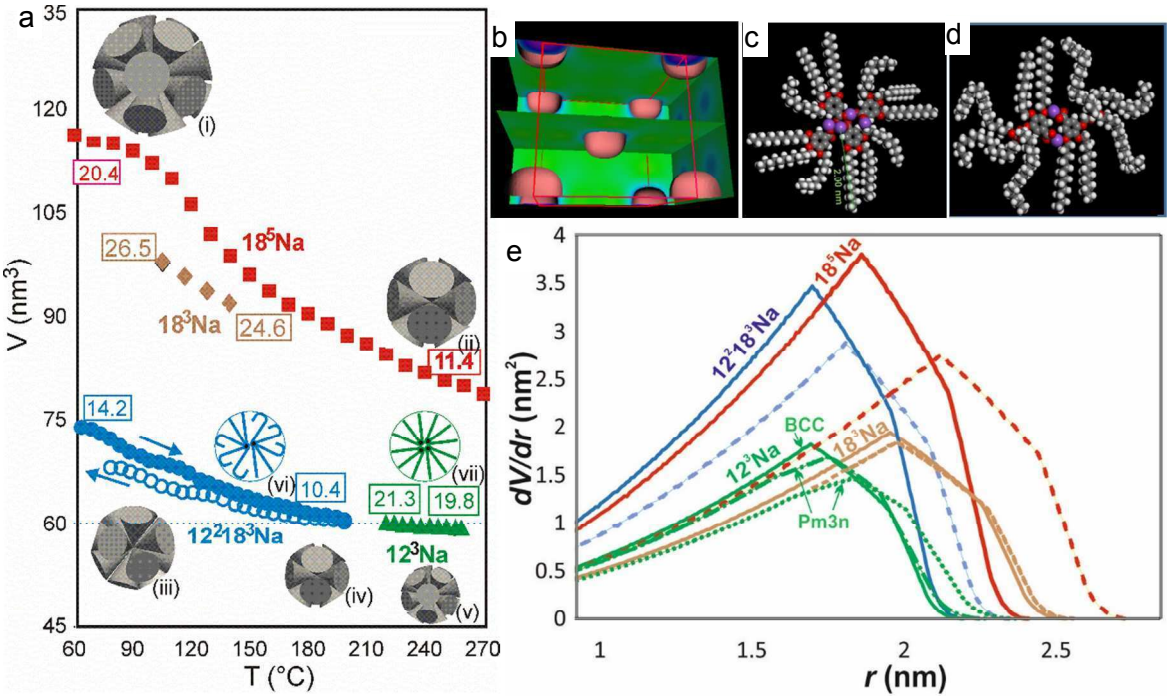

Figure 3. (a) Unit cell volume *vs.* temperature in the BCC phase for the compounds studied. Empty circles refer to a cooling run, full symbols are for heating. Numbers in boxes are numbers of molecules in a sphere (μ) at the low- and high-*T* ends of the associated curves. Insets are described in the text. (b) Electron density map of the BCC phase of compound **$12^2 18^3$Na**. The unit cell is delineated by the red cube. Orange isosurface encloses the spherical regions of high electron density, i. e. the aromatic cores and the ionic part. The colours on the walls and on the z = ½ "shelf" are: green = low (aliphatic), blue-purple = high (aromatic). The structure factor phase angles used are: $\phi_{110} = 0$, $\phi_{200} = \pi$, $\phi_{110} = 0$, $\phi_{211} = 0$. (c,d) CPK models of four molecules of (c) 12^3Na and (d) two molecules of **$12^2 18^3$Na** in a plane representing a likely arrangement in the cross-section of a column (columnar phase) or a sphere (cubic phase). Red = oxygen, purple = sodium. (e) Calculated *dV/dr* curves for the studied compound in the BCC phase and, for 12^3Na, also for the $Pm\bar{3}n$ phase. Here real volume gradients are plotted against real *r* , based on volume and μ data in (a). Dashed and solid curves refer, respectively, to the lowest and highest temperatures of the ranges displayed in (a). Dotted and dot-dash curves are for the $Pm\bar{3}n$ phase of **123Na**.

The thermal shrinkage of the spheres does not imply volume shrinkage of the material. As the compounds are made up mainly of alkyl chains, we have assumed the thermal expansivity to be close to that of liquid n-alkane $C_{16}H_{34}$.[42] Estimating the density at room

temperature to be approximately 0.95 g.cm^{-3} based on previous measurements,[36,35] and using the measured cell volumes and computed densities (see SI, Tables S3 and S4), we calculated μ, the number of molecules per sphere, at the low and high ends of the measured BCC range for all compounds studied – see numbers in boxes in Figure 3a. The spheres made up of the appropriate numbers of cones are schematically shown as insets (i) to (v) in Figure 3a. As *T* increases the surplus dendrons are evidently continuously expelled from the spherical micelles, while at the same time new micelles are formed from the ejected molecules. The largest drop in μ occurs in **18^{5}Na**, from 20.4 to 11.4. A similarly high rate of dendron ejection is also seen in **18^{5}Na.** This complex process of disassembly and reassembly of micelles is reversible, as illustrated by the data on unit cell expansion on cooling for **12^{2}18^{3}Na** (empty circles in Figure 3a). Some hysteresis is evident at the relatively high applied cooling rate (10 K.min^{-1}). The re-integration of dendrons on cooling is a somewhat slower process than that of their ejection and regrouping on heating.

Thermal contraction of the unit cell has been observed, and ejection of surplus dendrons postulated, also in the case of the columnar phase.[43,35,38] However in that case contraction is only two-dimensional, and one needs to ascertain that a compensating expansion along the column axis does not occur. In fact, when dendrons were covalently attached to a polymer backbone and prevented from leaving the column, the macroscopic fibre has been found to extend longitudinally on heating, in contrast to the usual longitudinal thermal shrinkage of polymer fibres.[43] In free minidendrons, where molecular spacing along the column axis was measured by X-rays, molecular ejection was confirmed as the most likely explanation of lateral shrinkage.[35,38] Nevertheless, there can be no better proof of continuous and reversible thermal disassembly and reassembly than is provided in the case of 3D cubic structures, where thermal shrinkage occurs along all three dimensions, and molecular ejection and reintegration is the only possible mechanism. The presently studied hyperbranched minidendrons provide so far the most compelling examples of this process.

In Figure 3e we show *dV/dr* curves in real scale (nm and nm^2 units) for the actual compounds studied here. As mentioned above, these curves represent the effective wedge shapes of rolled-out molecules (inset β in Figure 1). Figure 3e shows graphically the actual widening and longitudinal contraction of the wedges on heating from the lowest (dashed curves) to the highest *T* (solid curves). These are particularly prominent in **18^{5}Na** and **18^{3}Na**. The curves for **12^{3}Na** also illustrate graphically the equivalent change occurring isothermally upon the transition from $Pm\bar{3}n$ to BCC (*cf.* dot-dash and solid green curves). Note that the end points of the curves in Figure 3e (the length of the wedge) is directly related to the height of the curves in Figure 3a. A further unexpected and counterintuitive finding revealed by Figures 3a,e is that the size of the micelles of **12^{2}18^3** is exactly the same as that of **12^{3}Na**, i.e. that the extra pentaerithritol branch with three long C18 chains replacing a single C12 chain made no difference to the length of the molecule and the size of the micelle. The reason can be gathered by comparing the solid blue and green curves in Figure 3e; it shows that all extra material in **12^{2}18^{3}Na** had gone into doubling the width of the wedge, rather than extending it. That suggests that the sphere diameter is determined by the shorter chains, the long chains presumably folding back, being highly conformationally disordered or partially interdigitated – see schematics in insets (vi) and (vii) in Figure 3a and molecular models in Figure 3c,d. This illustrates how the molecular conformation adapts to the space filling requirement of the superstructure.

We note that although the *dV/dr* curves give a compelling rationale for many observed features of sequence, structure and size of micellar dendron phases, they should not be considered as the only factors involved. However, it is conspicuous that even if the differences in *dVdr* functions are rather subtle, as e.g. for BCC and $Pm\bar{3}n$ phases, in all compounds where both phases appear, the BCC is invariably the high-*T* phase. Such a clear-cut distinction does

not exist between the $Pm\bar{3}n$ and the tetragonal σ-phase, where the *dVdr* functions are very similar indeed.[1,35,36]

CONCLUSIONS

We have prepared the first examples of "hyperbranched minidendrons" of the AB_5 type and shown that the BCC structure provides what seems to be the ultimate mode of thermotropic spherical assembly for highly divergent dendrons. The *dV/dr*-based analysis was shown to be very useful in rationalizing the observed phase behaviour. Thermal shrinkage of supramolecular aggregates via molecular ejection and reassembly has been confirmed beyond doubt, with an unprecedented extent of shrinkage recorded in the **18^5Na** compound. The unexpected behaviour of minidendron **$12^2 18^3$Na** with mixed longer and shorter chains, forming micelles of exactly the same size as **12^3Na**, is attributed to back-folding of the added long chains. The results help improve our general understanding of the complex self-assembly behavour of taper-shaped molecules. We also believe that producing highly divergent dendrons like the hyperbranched ones in this study will allow larger guest molecules to be encapsulated into spherical dendron-based shells.

Acknowledgements. We acknowledge funding from NFSC China (21274132, 21544009), Zhejiang Natural Science Foundation (LY15B020007), Science Foundation of Zhejiang Sci-Tech University (14062016-Y), the joint NSF-EPSRC PIRE program "RENEW" (EP/K034308) and the Leverhulme Trust (RPG-2012-804). G.U. and L. C. are grateful, respectively, for the awards of State Specially Recruited Expert, and High-End Foreign Expert, both from the Government of China. For help with synchrotron SAXS experiments we thank Prof. N. Terrill at I22, Diamond Light Source, UK.

REFERENCES

[1] B. M. Rosen, C. J. Wilson, D. A. Wilson, M. Peterca, M. R. Imam and V. Percec, *Chem. Rev.*, 2009, **109**, 6275-6540.
[2] B. Donnio, S. Buathong, I. Bury and D. Guillon, *Chem. Soc. Rev*. 2007, **36**, 1495–1513.
[3] C. Tschierske, *Angew. Chem. Int. Ed*. 2013, **52**, 8828-8878.
[4] T. Kato, N. Mizoshita and K. Kishimoto, *Angew. Chem., Int. Ed*. 2006, **45**, 38–68.
[5] H.-J. Sun, S. Zhang and V. Percec, *Chem. Soc. Rev.* 2015, **44**, 3900-3923.
[6] F. Würthner, C. Thalacker, S. Diele and C. Tschierske, *Chem. Eur. J.* 2001**, 7**, 2245-2253.
[7] Z. An, J. Yu, B. Domercq, S. C. Jones, S. Barlow, B. Kippelen and S. R. Marder, *J. Mater. Chem.* 2009**, 19**, 6688-6698.
[8] G. Ungar, S. V. Batty, V. Percec, J. Heck and G. Johansson, *Adv. Mater. Opt. Electro*. 1994, **4**, 303–313.
[9] T. Ichikawa, M. Yoshio, A. Hamasaki, T. Mukai, H. Ohno and T. Kato, *J. Am. Chem. Soc.* 2007, **129**, 10662–10663.
[10] M. Peterca, V. Percec, A. E. Dulcey, S. Nummelin, S. Korey, M. Ilies and P. A. Heiney, *J. Am. Chem. Soc.* 2006, **128**, 6713–6720.
[11] C. S. Pecinovsky, E. S. Hatakeyama and D. L. Gin, *Adv. Mater.* 2008, **20**, 174–178.
[12] B. Soberats, M. Yoshio, T. Ichikawa, X. B. Zeng, S. Taguchi, H. Ohno, F. Liu, G. Ungar and T. Kato, *J. Am. Chem. Soc.* 2015, **137***,* 13212-13215.
[13] G. Johansson, V. Percec, G. Ungar and D. Abramic, *J. Chem. Soc., Perkin Trans. 1* **1994**, 447-459.

[14] A. Schultz, S. Laschat, A. Saipa, F. Gießelmann, M. Nimtz, J. L. Schulte, A. Baro and B. Miehlich, *Adv. Funct. Mater.* 2004, **14**, 163-168.
[15] V. Percec, M. Glodde, T. K. Bera, Y. Miura, I. Shiyanovskaya, K. D. Singer, V. S. K. Balagurusamy, P. A. Heiney, P. A.; Schnell, I.; Rapp, A.; Spiess, H.-W.; Hudson, S. D.; Duan, H. *Nature* **2002**, *419*, 384-388.
[16] X.-H. Zhang, A. Grant, S. Ellinger, S. A. Odom, D. Sweat, D. B. Tanner, A. G. Rinzler, S. Barlow, J.-L. Bredas, B. Kippelen, S. R. Marder and J. R. Reynolds, *J. Am. Chem. Soc.* 2009, **131**, 2824-2826.
[17] D. J. P. Yeardley, G. Ungar, V. Percec, N. M. Holerca and G. Johansson, *J. Am. Chem. Soc.*, 2000, **122**, 1684-1689.
[18] Y. Tsuda, R. Kuwahara and J.-M. Oh, *Trans. Mater. Res. Soc. Jpn.* **2004**, *29*, 267-271.
[19] A. Grotzky, E. Atamura, J. Adamcik, P. Carrara, P. Stano, F. Mavelli, T. Nauser, R. Mezzenga and A. D. Schluter, *Langmuir* 2013, **29***,* 10831-10840.
[20] V. Percec, A. E. Dulcey, M. Peterca, P. Adelman, R. Samant, V. S. K. Balagurusamy and P. A. Heiney, *J. Am. Chem. Soc.* 2007, **129**, 5992-6002.
[21] B. Donnio, P. Garcia-Vazquez, J.-L. Gallani, D. Guillon and E. Terazzi, E. *Adv. Mater*. 2007, **19**, 3534-3539.
[22] K. Kanie, M. Matsubara, X. B. Zeng, F. Liu, G. Ungar, H. Nakamura and A. Muramatsu, A. *J. Am. Chem. Soc.*, 2012, **134***,* 808-811.
[23] X. Feng, M. E. Tousley, M. G. Cowan, B. R. Wiesenauer, S. Nejati, Y. Choo, R. D. Noble, M. Elimelech, D. L. Gin and C. O. Osuji, *ACS Nano*, 2014, **8**, 11977–11986.
[24] G. Ungar, F. Liu and X.B. Zeng, "Thermotropic Cubic Liquid Crystal Phases, Other 3D Phases and Quasicrystals" Chap. 7 in **Handbook of Liquid Crystals,** 2nd Ed., Vol. 5, J.W. Goodby, P.J. Collings, T. Kato, C. Tschierske, H.F. Gleeson, P. Raynes eds., VCH_Wiley, Weinheim, 2014, 363-436.
[25] B. P. Hoag and D. L. Gin, *Liq. Cryst.* 2004, **31**, 185-199.
[26] B.-K. Cho, A. Jain, S. M. Gruner and U. Wiesner, *Science*, 2004, **305**, 1598-1601.
[27] P. Ziherl, and R. D. Kamien, *J. Phys. Chem. B*, 2001, **105**, 10147-10158.
[28] Y. Y. Li, S. T. Lin and W. A. Goddard, W. A. *J. Am. Chem. Soc.*, 2004, **126**, 1872-1885.
[29] G. Ungar and X. B. Zeng, *Soft Matter*, 2005, **1**, 95-106.
[30] V. S. K. Balagurusamy, G. Ungar, V. Percec and G. Johansson, *J. Am. Chem. Soc.*, 1997, **119,** 1539-1555.
[31] K. Borisch, S. Diele, P. Göring, H. Müller and C. Tschierske, *Liq. Cryst.*, 1997, **22,** 427-443.
[32] G. Ungar, Y. S. Liu, X. B. Zeng, V. Percec and W. D. Cho, *Science*, 2003, **299**, 1208-1211.
[33] C. H. M. Weber, F. Liu, X. B. Zeng, G. Ungar, N. Mullin, J. K. Hobbs, M. Jahr and M. Lehmann, *Soft Matter*, 2010, **6**, 5390–5396.
[34] X. B. Zeng, Y. S. Liu, G. Ungar, V. Percec , A. E. Dulcey and J. K. Hobbs, *Nature***,** 2004, **428,** 157-160.
[35] G. Ungar, V. Percec, M. N. Holerca, G. Johansson and J. A. Heck, *Chem. Eur. J*., 2000, **6**, 1258-1266.
[36] V. Percec, M. N. Holerca, S. Uchida, W.-D. Cho, G. Ungar, Y. Lee and D. J. P. Yeardley, *Chem. Eur. J.*, 2002, **8**, 1106-1117.
[37] U. Beginn, L. Yan, S. N. Chvalun, M. A. Shcherbina, A. Bakirov and M. Möller, *Liq. Cryst*. 2008, **35**, 1073-1093.
[38] M.-H. Yen, J. Chaiprapa, X. B. Zeng, Y. S. Liu, L. Cseh, G. H. Mehl and G. Ungar, *J. Am. Chem. Soc.* 2016, **138**, 5757–5760.
[39] K. Kanie, M. Matsubara, X. B. Zeng, F. Liu, G. Ungar, H. Nakamura and A. Muramatsu, *J. Am. Chem. Soc.*, 2012, **134**, 808-811.
[40] G. Zerbi, R. Magni, M. Gussoni, K. H. Moritz, A. Bigotto and S. Dirlikov, *J. Chem. Phys.* 1981, **75**, 3175-3194.

[41] We note that some reduction in unit cell volume has also been observed on heating the bicontinuous cubic LC phases – see S. Kutsumizu, H. Mori, M. Fukatami, S. Naito, K. Sakajiri and K. Saito, *Chem. Mater.* 2008, **20**, 3675-3687. However in that case the cause of the contraction is more complex as thermal increase in twist angle between successive molecular layers tends to shorten the distance between network junctions, causing additional unit cell contraction – see C. Dressel, F. Liu, M. Prehm, X.B. Zeng, G. Ungar and C. Tschierske *Angew. Chem. Int. Ed.,* 2014, **53**, 13115 –13120.

[42] R. A. Orwoll and P. J. Flory, *J. Am. Chem. Soc.* 1967, **89**, 6814-6822.

[43] J.-K. Kwon, S. N. Chvalun, J. Blackwell, V. Percec and J. A. Heck, *Macromolecules* 1995, **28**, 1552-1558.

Conceptual insights:

While there is vast literature, and even a Nobel prize, on understanding how rod-like mesogens form nematic and smectic liquid crystal phases, there is remarkably little on understanding physical principles of self-assembly of tapered, or wedge-shaped mesogens, even though experimentally accumulated information has now become very substantial. Tapered molecules, including dendrons, form primarily columnar and cubic mesophases and, on their own or attached to other functional molecular moieties, they probably account for the majority of thermotropic self-assembled systems today. Virtually all design of such compounds has so far been empirically based. In contrast, here we use an approach based on a quantitative geometrical model that relates the shape of the molecules and the mode of their self-assembly. The model prompted us to prepare “hyperbranched” minidendrons with the shape of highly divergent “exponential” wedge. They were found to display the body-centred cubic mesophase. This appears to be the ultimate thermotropic assembly mode of highly divergent wedges. The compounds indeed assemble as the model predicts, and disassemble and reassemble thermally in a way compatible with the model. Among other outcomes of this work, the adopted principle of highly divergent wedges should help obtain better vehicles for encapsulation of different molecular species.

Table of Contents entry

Body-centred cubic packing of spheres – The ultimate thermotropic assembly mode for highly divergent dendrons

Xiaohong Yao[1], Liliana Cseh[1,2], Xiangbing Zeng[3], Min Xue[1], Yongsong Liu[1], Goran Ungar[1,3,*]

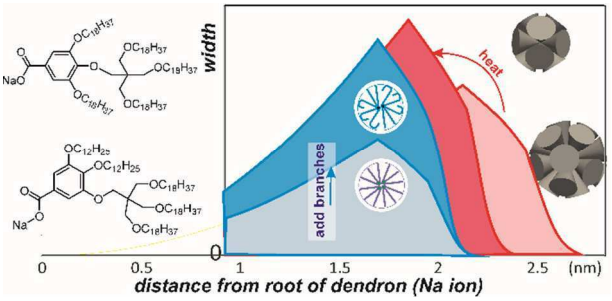

Text:
Na salts of benzoic acid carrying five long alkoxy chains (“hyperbranched” AB5 minidendrons) self-assemble into spheres which shrink to half their size on heating and display chain back-folding, obeying the predictions of the proposed geometrical model of self-assembly of taper-shaped molecules.

Supplementary Information

Body-centred cubic packing of spheres – The ultimate thermotropic assembly mode for highly divergent dendrons

Xiaohong Yao[1], Liliana Cseh[1,2], Xiangbing Zeng[3], Min Xue[1], Yongsong Liu[1], Goran Ungar[1,3,*]

[1]Department of Physics, Zhejiang Sci-Tech University, Xiasha College Park, Hangzhou 310018, China

[2]Institute of Chemistry, Timisoara of Romanian Academy, Timisoara – 300223, Romania

[3]Department of Materials Science and Engineering, University of Sheffield, Sheffield S1 3JD, U.K.

Contents

Techniques

Chemical analysis and DSC. ^{1}H-NMR spectra were recorded on a Bruker Advance II DMX 400 spectrometer and ^{13}C-NMR spectra were recorded on a Bruker Advance III 500 spectrometer using $CDCl_3$ as solvent and TMS as internal standard. Chemical shifts are reported as ppm. The purity of products was determined by a combination of techniques including thin-layer chromatography (TLC) on silicagel-coated aluminum plates and elemental analysis system VarioMICRO cube from Elementar Analysensysteme. High-resolution mass spectrometry experiments were performed with a Bruker Daltonics Apex III spectrometer or with a Bruker 7-Tesla FT-ICR mass spectrometer equipped with an electrospray source (Billerica,

MA, USA). Thermal transitions of samples were measured on a TA Instruments Q200 and Mettler differential scanning calorimeter (DSC) with 10°C min^{-1} heating and cooling rates. The samples were dried *in vacuo* at room temperature for 1-2 days prior to the scan, and the DSC cell was flushed with dry nitrogen. First order transition temperatures were reported as the maxima and minima of their endothermic and exothermic peaks, corrected for thermal lag determined from the ascending slope of indium melting endotherm at the appropriate heating rate. Indium was also used to calibrate temperature and heat flow.

X-ray diffraction. Small-angle X-ray diffraction (SAXD) experiments on liquid crystal phases were performed by using both a laboratory X-ray source and synchrotron radiation. The laboratory set-up consisted of a Xenocs microfocus copper source, a Fox3d infinity focussing multilayer mirrors and a collimator containing scatterless Si slits. The detector was a Mar 345 image plate detector, positioned off-centre, 1.3 m from the sample. Primary and scattered beam tubes were evacuated. Synchrotron SAXD experiments were carried out on beamline I22 at Diamond Light Source, UK, using a Pilatus detector bank. In both set-ups the samples were kept in 1 mm X-ray capillaries held in a Linkam hot stage with a bore for the capillary and mica windows to prevent convection. As with the DSC measurements, the samples for X-ray were also dried *in vacuo* at room temperature for 1-2 days prior to the experiment. Immediately on transferring them to the capillaries, the capillaries were evacuated on a vacuum line and sealed. Azimuthally averaged radial scans of scattered intensity were obtained using Fit2d and Fibrefix. 3-D electron density maps were reconstructed as described elsewhere. [S1] Wide-angle X-ray diffraction was recorded using a Rigaku rotating anode generator with Osmic multilayer mirrors and a Mar 345 image plate detector. A Cryostream N_2 jet was used to control the sample temperature.

Materials

All reagents used were of analytical grade and were purchased from Enerrgy or Aladdin Chemicals. THF was dried by distillation on Na/benzophenone. The other solvents were used without further purification other than drying over molecular sieves.

Methyl 4-(benzyloxy)-3,5-dihydroxybenzoate **(2)** was obtained according to ref. S2, methyl 3,4-bis(dodecyloxy)-5-hydroxy-benzoate **(7)** according to ref. [3] and sodium 3,4,5-trialkoxybenzoate (**12** and **13**) according to ref. S4. The procedure used for the preparation of 3-(octadecyloxy)-2,2-bis((octa-decyloxy)methyl)propan-1-ol **(1)** is an improvement on the previous method [S5].

Abreviations: DCM – dichloromethane; DIAD - diisopropyl azodicarboxylate; DMF – dimethylformamide; EtOAc – ethyl acetate; PE – petroleum ether (fraction 60-90); THF – tetrahydrofurane; TBAB - tetrabuthylammonium bromide.

Syntnthetic schemes

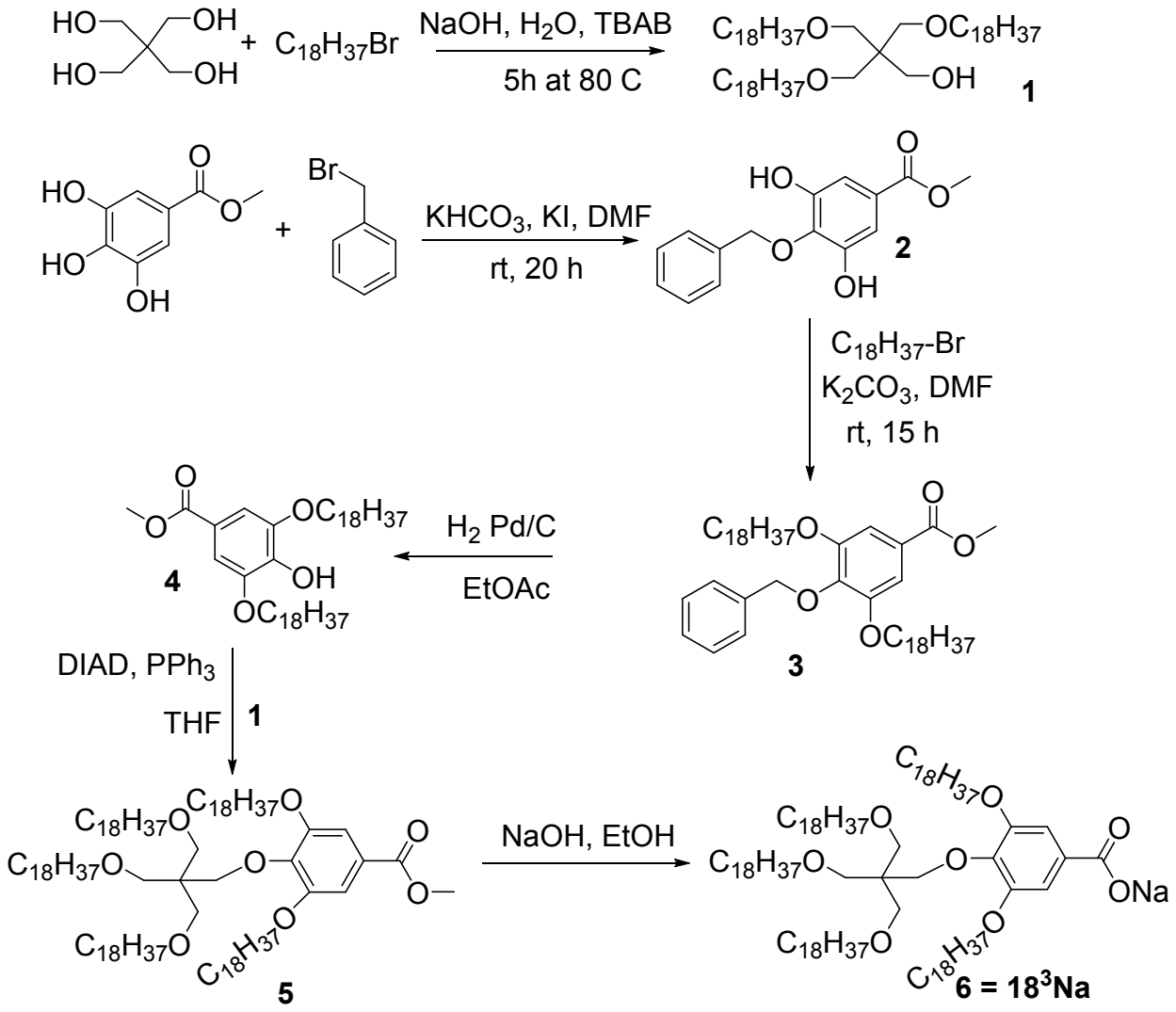

Scheme S1. Synthesis of the carboxylate sodium salt **18^5Na**

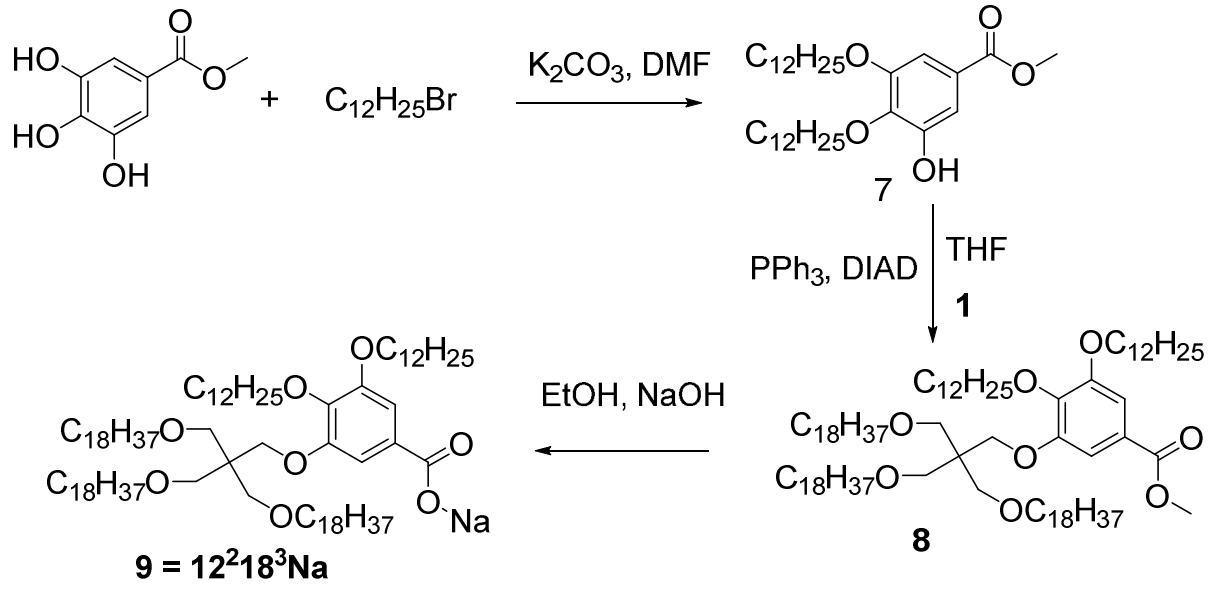

Scheme S2. Synthesis of the carboxylate sodium salt **$12^2 18^3$Na**

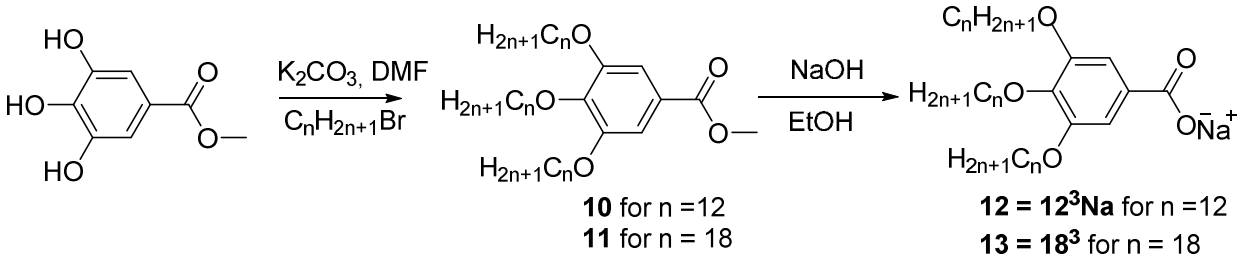

Scheme S3. Synthesis of sodium 3,4,5-trialkoxybenzoates **12^3Na** and **18^3Na**

Synthesis and characterization of compounds

3-(octadecyloxy)-2,2-bis((octa-decyloxy)methyl)propan-1-ol **(1)** A solution of sodium hydroxide (80 g, 2.0 mol) in water (125 mL) was heated at 80 ºC, pentaerythritol (6.3 g, 46 mmol) was added and stirred at this temperature for 30 min. TBAB (6.5 g, 0.020 mol) and then 1-bromooctadecane (66.7 g, 0.20 mol) were added. The mixture was stired at 80 ºC for other 5 hours. The solution was cooled down at 50 ºC and $CHCl_3$ (200 ml) was added. The organic layer was separated, cooled down at r. t., acidulated with HCl 0.1 N until pH = 5, washed with H_2O and dried over $MgSO_4$ anhydrous. The solvent was removed and the crude product was purified by column chromatography (SiO_2, PE and then PE/EtOAc = 9/1) (Rf = 0.57 for PE/EtOAc = 9/1). The pure product was obtained as a yellow-white solid (10.2 g, 24 % yield).

^{1}H-NMR (400 MHz, $CDCl_3$, r.t) δ (ppm): 3.70 (d, 2H, HO-C**H_2**-, *J* = 5.6 Hz), 3.43 (s, 6H, -C-(C**H_2**-O-$C_{18}H_{37})_3$), 3.38 (t, 6H, -C-(CH_2-O-C**H_2**-$C_{17}H_{35})_3$, *J* = 6.5 Hz), 3.18 (t, 1H, -OH, *J* = 5.9 Hz), 1.53 (m, 6H, (-O-CH_2-C**H_2**-$C_{16}H_{33})_3$), 1.25 (m, 90H, -CH_2-), 0.88 (t, 9H, - CH_3, *J* = 6.4 Hz).

^{13}C-NMR (125 MHz, $CDCl_3$, r.t.) δ (ppm): 71.8, 71.5, 66.6, 44.7, 31.9, 30.9, 29.3-29.7, 26.2, 22.7, 14.1.

Methyl 4-(benzyloxy)-3,5-bis(octadecyloxy)benzoate (**3**): To a solution of diol **2** (5.48 g, 20 mmol) and potassium carbonate (6.91 g, 50 mmol) in DMF (100 mL) 1-bromooctadecane (16.67 g, 50 mmol) was added. The mixture was stirred for 20 hours at r.t. The precipitate was filtered. The DMF was distilled off and the crude product was dissolved in EtOAc (30 ml). The organic phase was washed with H_2O and dried over $MgSO_4$ anhydrous. The solvent was removed and the crude product was purified by column chromatography (SiO_2, DCM/PE = 1/1, Rf = 0.47) to afford a white solid (1.02 g, 7 % yield).

^{1}H-NMR (400 MHz, $CDCl_3$, r.t.) δ (ppm): 7.49 (d, 2H, Har, J = 7.44 Hz), 7.37-7.27 (m, 3H, Har), 7.26 (s, 2H, Har), 5.08 (s, 2H, -C**H$_2$**-C_6H_5), 4.01 (t, 4H, –O-CH_2-, J = 6.4 Hz), 3.89 (s, 3H, -COO-CH_3), 1.81 (q, 4H, -O-CH_2-C**H$_2$**-), 1.47 (q, 4H, -CH_2-), 1.21-1.40 (overlap, 32H, -CH_2-), 0.88 (t, 6 H, -CH_2-C**H$_3$**, J = 6.0 Hz).

^{13}C-NMR (125 MHz, $CDCl_3$, r.t.) δ (ppm): 166.8, 152.6, 141.5, 137.6, 128.1, 127.6, 124.9, 107.7, 74.8, 69.1, 52.1, 31.9, 30.9, 29.3-29.6, 26.1, 22.7, 14.1.

Methyl 4-hydroxy-3,5-bis(octadecyloxy)benzoate (**4**). 10% Pd/C (0.30 g) was added to a solution of compound **3** (2.0 g, 2.6 mmol) in EtOAc (20 mL) and the mixture was stirred under hydrogen for 2 hours. The reaction mixture was filtered and the solvent was evaporated. The product was obtained as a white solid (1.6 g, 90% yield).

^{1}H-NMR (400 MHz, $CDCl_3$, r.t.) δ (ppm): 7.28 (s, 2H, Har), 5.88 (s, 1H, -OH), 4.07 (t, 4H, -O-CH_2-), 3.88 (s, 3H, -COO-CH_3), 1.83 (m, 4H, -O-CH_2-C**H$_2$**-), 1.45 (m, 4H, -CH_2-), 1.25 (m, 60H, -CH_2-), 0.88 (t, 6 H, -CH_3, J = 6.4 Hz).

^{13}C-NMR (125 MHz, $CDCl_3$, r.t.) δ (ppm): 167.0, 145.1, 139.8, 120.9, 107.7, 69.5, 52.0, 31.9, 30.9, 29.6-29.7, 29.5-29.6, 29.3, 29.2, 25.9, 22.6, 14.1.

Methyl 3,5-bis(octadecyloxy)-4-(3-(octadecyloxy)-2,2-bis((octadecyloxy)methyl) propoxy)benzoate (**5**). To compound **4** (0.37 g, 0.50 mmol), pentaerythritol derivative **1** (0.47 g, 0.53 mmol) and PPh_3 (0.14 g, 0.53 mmol) in dry THF (1 ml) was added drop wise DIAD (0.32 ml 1.62 mmol) under nitrogen at 67 °C. The reaction was refluxed for 4 hours. The solvent was removed and the crude product was dissolved in DCM. The mixture was washed successively with water, NH_4Cl (2 × 50 ml), brine (2 × 20 ml), water and dried over by $MgSO_4$. The solvent was evaporated under pressure and the product was purified by chromatography (SiO_2, DCM/PE = 1/1, Rf = 0.68) to give an white solid (0.57 g, 38% yield).

LRESIMS: *m*/*z* calcd. for $[M + Na]^+$ $C_{103}H_{198}NaO_8$, 1586.4984, found 1586.4978, error 0.4 ppm.

^{1}H-NMR (400 MHz, $CDCl_3$, r.t.) δ (ppm): 7.22 (s, 2H), 4.13 (s, 2H), 3.98 (t, 4H, J = 6.4 Hz), 3.87 (s, 3H), 3.54 (s, 6H), 3.35 (t, 6H, J = 6.5Hz), 1.81 (m, 4H), 1.48 (m, 10H), 1.25 (m, 90H), 0.88 (t, 15 H, J = 6.4Hz).

^{13}C-NMR (125 MHz, $CDCl_3$, r.t.) δ (ppm): 167.0, 152.2, 143.0, 124.0, 107.9, 73.1, 71.5, 69.6, 69.1, 52.0, 45.9, 31.9, 30.9, 29.6-29.7, 29.4-29.5, 26.2, 26.1, 22.7, 14.1.

Sodium 3,5-bis(octadecyloxy)-4-(3-(octadecyloxy)-2,2-bis((octadecyloxy)methyl) propoxy)benzoate (**6**). A mixture of **5** (1.2 g, 0.77 mmol), NaOH (0.18 g, 4.5 mmol) and 90% EtOH (50 ml) was refluxed for 10 hours. After cooling to r.t., the resulting precipitate was filtered off. The compound was purified by recrystallization five times from EtOH (90%) as a white powder (1.1 g, 92 %).

MS: *m*/*z* calcd. for $[M + H]^+$ $C_{102}H_{195}O_8Na$, 1572.47, found 1572.48; Anal. Calcd. For $C_{102}H_{195}O_8Na \cdot H_2O$: C 77.02, H 12.48; found: C 76.90, H 12.28.

^{1}H-NMR (400 MHz, $CDCl_3$, r.t.) δ (ppm): 7.11 (s, 2H), 3.98 (s, 4H), 3.81 (t, 4H), 3.54 (s, 6H), 3.35 (t, 6H, *J* = 6.5 Hz), 1.81 (m, 4H), 1.48 (m, 10H), 1.25 (m, 90H), 0.88 (t, 15 H, *J* = 6.3Hz).

Methyl 3,4-bis(dodecyloxy)-5-(3-(octadecyloxy)-2,2-bis((octadecyloxy)methyl) propoxy)benzoate (**8**). The method of synthesis is the same as for **5**. The crude product was purified by column chromatography (SiO_2, DCM/PE = 1/1, Rf = 0.63) to give an white solid (0.45 g, 36 % yield).

MS: *m*/*z* calcd. for $[M + Na]^+$ $C_{91}H_{174}NaO_8$:1419.39, found 1419.31.

^{1}H-NMR (400 MHz, $CDCl_3$, r.t.) δ (ppm): 7.28 (s, 1H), 7.23 (s, 1H), 3.98 (m, 6H) 3.97 (s, 3H), 3.50 (s, 6H), 3.36 (t, 6H, *J* = 6.3Hz), 1.8 (m, 4H), 1.49 (m, 10H), 1.25 (m, 84H), 0.88 (t, 15H, *J* = 6.3Hz).

^{13}C-NMR (125 MHz, $CDCl_3$, r.t.) δ (ppm): 14.1, 22.7, 26.2, 26.1, 29.3-29.6, 30.2, 30.5, 31.0, 31.4, 32.0, 45.4, 52.0, 68.2, 69.0, 69.4, 71.6, 73.4, 107.6, 107.9, 124.7, 142.1, 152.7, 153.0, 166.9 .

Sodium 3,4-bis(dodecyloxy)-5-(3-(octadecyloxy)-2,2-bis((octadecyloxy)methyl) propoxy)benzoate (**9**). The method of synthesis is the same as for **6.**

MS: *m*/*z* calcd. for $[M + H]^+$ $C_{90}H_{172}O_8Na$: 1404.34, found: 1405.30; Anal. Calcd. For $C_{90}H_{171}O_8Na \cdot H_2O$: C 76.00, H 12.26; found: C 76.04, H 12.19.

^{1}H-NMR (400 MHz, $CDCl_3$, r.t.) δ (ppm): 7.24 (s, 1H), 7.19 (s, 1H), 3.96 (m, 6H), 3.51 (s, 6H), 3.35 (t, 6H, *J* = 6.4 Hz), 1.73 (m, 4H), 1.27 (m, 84H), 0.90 (t, 15H, *J* = 6.2 Hz).

DSC thermograms

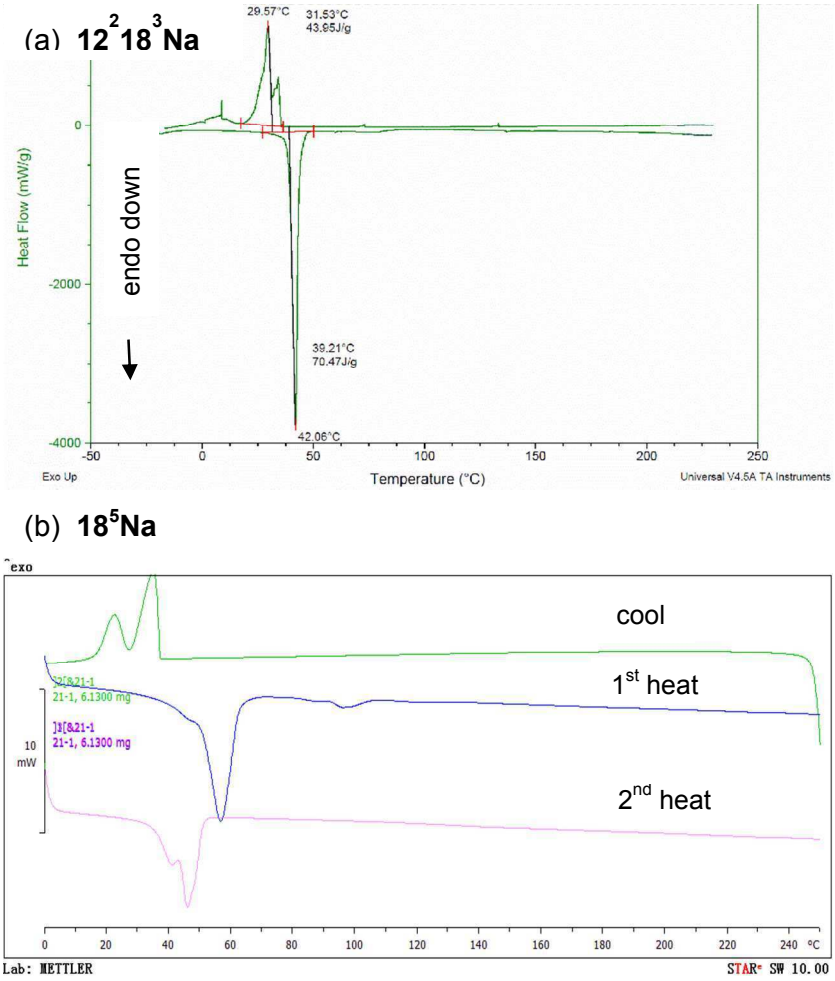

Figure S1. DSC thermograms of (a) 12^{2}**18^{5}Na**, (b) **18^{5}Na.** Heating and cooling rates are 10 K min^{-1}.

Additional X-ray diffraction data

SAXS diffractograms

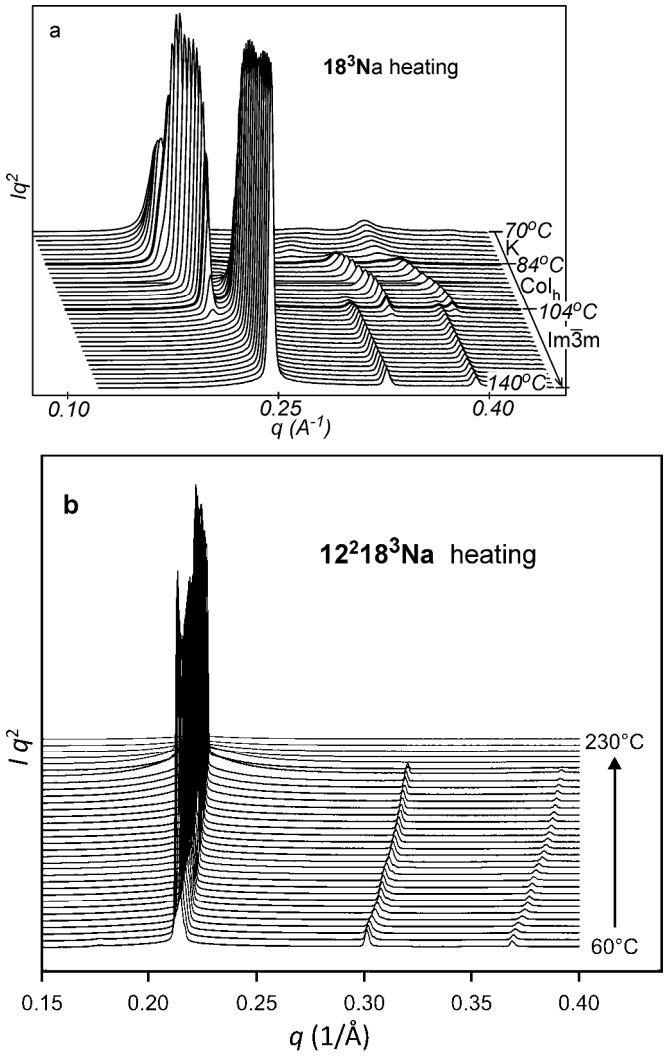

Figure S2. Small-angle X-ray diffractograms recorded during heating of compounds (a) **18^3Na** and (b) **$12^2 18^3$Na**.

Measured spacings, lattice parameter and unit cell volume vs. temperature

As an example we list all measured Bragg spacings from the small-angle X-ray diffractograms as a function of temperature recording on heating and cooling for compound **$12^2 18^3$Na** on heating and cooling (results from synchrotron experiments).

Table S1. Measured d-spacings of the (110), (200) and (211) diffraction peaks of the BCC phase, lattice parameter *a* and unit cell volume V, for compound **$12^2 18^3$Na** on heating.

T (°C)	$d_{(110)}$	$d_{(200)}$	$d_{(211)}$	*a* (nm)	V (nm^3)
60	2.944	2.083	1.700	4.17	72.26
65	2.937	2.080	1.696	4.16	71.80
70	2.931	2.077	1.694	4.15	71.44
75	2.922	2.070	1.688	4.14	70.74
80	2.909	2.061	1.679	4.12	69.73
85	2.899	2.051	1.675	4.10	69.01
90	2.893	2.042	1.668	4.09	68.28
95	2.887	2.039	1.664	4.08	67.88
100	2.880	2.035	1.662	4.07	67.50
105	2.874	2.033	1.658	4.06	67.13
110	2.868	2.029	1.656	4.06	66.78
115	2.859	2.024	1.650	4.04	66.13
120	2.850	2.014	1.646	4.03	65.43
125	2.838	2.008	1.640	4.02	64.74
130	2.832	2.002	1.636	4.00	64.23
135	2.825	1.999	1.632	4.00	63.84
140	2.820	1.993	1.628	3.99	63.38
145	2.814	1.990	1.624	3.98	63.01
150	2.808	1.985	1.622	3.97	62.63
155	2.801	1.981	1.618	3.96	62.19
160	2.796	1.978	1.614	3.96	61.87
165	2.794	1.975	1.613	3.95	61.66
170	2.790	1.974	1.611	3.95	61.47
175	2.784	1.970	1.608	3.94	61.09
180	2.779	1.967	1.606	3.93	60.81
185	2.776	1.963	1.604	3.93	60.59
190	2.773	1.960	1.602	3.92	60.35
195	2.767	1.958	1.595	3.91	59.85

Table S2. Measured d-spacings of the (110), (200) and (211) diffraction peaks of BCC phase, lattice parameter *a* and unit cell volume V, of compound **$12^2 18^3$Na** on cooling.

T (°C)	$d_{(110)}$	$d_{(200)}$	$d_{(211)}$	*a* (nm)	V (nm^3)
80	2.881	2.047	1.664	4.08	67.99
85	2.881	2.045	1.664	4.08	67.95
90	2.881	2.042	1.663	4.08	67.78
95	2.878	2.039	1.662	4.07	67.57
100	2.876	2.037	1.660	4.07	67.38
105	2.874	2.035	1.656	4.06	67.12
110	2.870	2.033	1.654	4.06	66.86
115	2.868	2.027	1.654	4.05	66.60
120	2.862	2.020	1.650	4.04	66.11
125	2.859	2.014	1.648	4.04	65.72
130	2.856	2.011	1.646	4.03	65.49
135	2.850	2.008	1.644	4.02	65.17
140	2.847	2.007	1.642	4.02	64.99
145	2.843	2.005	1.638	4.01	64.68
150	2.840	2.002	1.636	4.01	64.48
155	2.838	1.999	1.634	4.00	64.21
160	2.834	1.996	1.632	4.00	63.96
165	2.832	1.995	1.628	3.99	63.70
170	2.825	1.993	1.626	3.99	63.41
175	2.823	1.990	1.622	3.98	63.13
180	2.820	1.987	1.620	3.98	62.89
185	2.814	1.981	1.618	3.97	62.48
190	2.810	1.978	1.616	3.96	62.24

Calculation of density and number of molecules per micelle

Table S3. Calculation of densities of $12^2 18^3$Na and 18^3Na at different temperatures

Temperature *T* (°C)	Expansivity of n-$C_{16}H_{37}$ [S6] α x 10^3 (deg^{-1})	at T (°C)	Relative volume expansion (v/v_{20})[b]	density (g cm^{-3}) (based on ρ_{20} = 0.95 g cm^{-3} at 20 °C)[S4]
20	0.897[a]			
160	1.092[a]			
200	1.200[a]			
40	0.911[b]	60	1.036	0.917
107.5	0.990[c]	195	1.173	0.810
145	1.060[d]	270	1.265	0.751

[a)]Thermal expansivity α of $C_{16}H_{37}$ at stated temperature from ref. S6.

[b)]Calculated using average expansivity $<\alpha_T>$ in the interval 20°C to *T*,.

Table S4. Number of molecules per sphere in the BCC phase (μ)

Compound	M (Da)	T (°C)	Unit cell volume V (nm^3)	density (ρ) ($g.cm^{-3}$)	μ
12^3Na	696	220	60.0	0.82	21.3
		258	59.4	0.765	19.8
18^3Na	948	104	94.9	0.884	26.5
		140	91.3	0.852	24.6
$12^2 18^3$Na	1402	60	72.2	0.917	14.2
		195	59.85	0.810	10.4
18^5Na	1570	60	116.2	0.917	20.4
		270	78.8	0.751	11.4

References

[S1] D.R. Dukeson, G. Ungar, V.S.K. Balagurusamy, V. Percec, G. Johansson and M. Glodde, *J. Am. Chem. Soc.* 2003, **125**, 15974-15980.
[S2] N. Michihata, Y. Kaneko, Y. Kasai, K. Tanigawa, T. Hirokane, S. Higasa and H. Yamada, *J. Org. Chem*., 2013, **78**, 4319-4328.
[S3] S. Yamaguchi, Y. Ashikaga, K. Nishii and H. Yamada, *Org. Lett*., 2012, **14**, 5928-5931.
[S4] V. Percec, M. N. Holerca, S. Uchida, W.-D. Cho, G. Ungar, Y. Lee and D. J. P. Yeardley, *Chem. Eur. J.*, 2002, **8**, 1106-1117.
[S5] Ajinomoto Co., Inc. Tokyo 104-8315 (JP), EP 2518041 A1, **2012**.
[S6] R. A. Orwoll and P. J. Flory, *J. Am. Chem. Soc.* 1967, **89**, 6814-6822.

Body-centred cubic packing of spheres – The ultimate thermotropic assembly mode for highly divergent dendrons

Xiaohong Yao[1], Liliana Cseh[1,2], Xiangbing Zeng[3], Min Xue[1], Yongsong Liu[1], Goran Ungar[1,3,*]

[1]Department of Physics, Zhejiang Sci-Tech University, Xiasha College Park, Hangzhou 310018, China
[2]Institute of Chemistry, Timisoara of Romanian Academy, Timisoara – 300223, Romania
[3]Department of Materials Science and Engineering, University of Sheffield, Sheffield S1 3JD, U.K.

Abstract

We have synthesised sodium tris(alkoxy)benzoates in which one of the three alkyl chains branches further into three $C_{18}H_{37}$ chains. These AB5 hyperbranched minidendrons melt directly into a body-centred cubic (BCC) mesophase formed by spherical "micelles". In contrast, their non-branched counterparts display various mesophases before they turn BCC on heating. This agrees with the predictions from a numerical geometric model that relates the shape of the molecular wedge to the type of mesophase they adopt. The spheres were found to shrink in volume on heating and expand on cooling, as molecules, in some cases nearly half of them, are ejected and again reintegrated in the spheres. The ejection of dendrons is caused by their lateral thermal expansion. The BCC appears to be the ultimate mesophase for the extremely divergent wedges such as the hyperbranched minidendrons. In dendrons with chains of unequal length, the sphere size is fixed by the shorter chains, the longer ones back-folding or interdigitating to effectively widen the wedge. The new understanding of their assembly will help design new dendrons, e.g. for better encapsulation of guest molecules.

Main text

Taper-shaped molecules that possess a degree of amphiphilicity often exhibit liquid crystal (LC) phases with 2-D or 3-D periodicity. The majority of such compounds so far have been dendrons and "minidendrons", typically containing an aromatic core and flexible terminal alkyl or oligo(ethylene oxide) chains.[1,2,3,4,5] Taper-shaped mesogens, including dendrons, are some of the most fundamental and widespread building blocks in supramolecular chemistry. They have been attached to moieties such as organic semiconductors,[6,7] ionic conductors,[8,9,10,11,12] crown ethers,[13,14] donor-acceptor complexes,[15,16] polymers,[17,18,19] peptides,[20] nanoparticles[21,22] etc. This way "dendronized" functional materials may be created that can be used in a variety of potential applications.[23] The most common supramolecular objects that such dendrons or dendronized compounds form are columns and spheres. When the tapered molecules are fan-shaped, i.e. when they can easily fit in a plane, the compound is likely to form a columnar phase. Oversimplified, the pizza-slice-like molecules self-assemble into disks ("pizzas") which, in turn, stack on top of each other and form columns which, finally, assemble on a 2-D lattice, usually hexagonal. However, if the peripheral chains have a cross-section larger than would fit in a plane, such tapered molecules adopt a conical shape. The cones then assemble into spheres which, in turn, pack on 3-D lattices.[24]

Fan shape induced columnar organization, often due to the attachment of alkoxyphenyl, or Percec-type dendrons,[1] can be usefully exploited in many ways, e.g. in forming 1-D electronic[6,7] and ionic [8,9,10,11,12] conductors, in encapsulating light-emitting polymers,[25] forming artificial ionic channels etc. Temperature-induced transition from columns to spheres can be used e.g. to create

a thermal switch, whereby an ionically or electronically conducting columnar molecular wire would split into isolated spherical fragments at a pre-set temperature and break the circuit.[26] Spherical assembly can also in principle be used to encapsulate and isolate molecules such as organic light emitters to prevent radiationless energy transfer. But this development has been hampered by high sensitivity of supramolecular thermotropic micelles to insertion of any larger entity at the thin end of the molecular wedge thereby effectively reducing the taper and reverting the spheres to columns. A better fundamental understanding of the spherical assembly of tapered molecules is keenly needed. There are also remarkably few theoretical or simulation studies on the subject.[27,28]

The lattices formed by the supramolecular spheres, or micelles, are the same as those found in metals and alloys, albeit on a length-scale an order of magnitude larger, with inter-sphere spacing typically of the order of 2-4 nm.[29] Wedge-shaped compounds have been found to exhibit the following micellar LC phases: the cubic phase with $Pm\bar{3}n$ symmetry and 8 spheres in a unit cell, known in metallurgy as A15;[30,31] the tetragonal $P4_2/mnm$ phase (the "σ-phase") with 30 spheres; [32] the body-centred cubic (BCC), space group $Im\bar{3}m$ and with only 2 spheres per cell;[17,33] and the aperiodic dodecagonal liquid quasicrystal (LQC).[34] Recently compiled statistics on the occurrence of these phases[24] based on the data in ref. 1 is summarized in Table 1. The $Pm\bar{3}n$ cubic phase is found to be by far the most common, observed in 84% of all appearances of micellar phases, and 55% of all LC phases detected in such compound, including columnar and smectic phases. On the other hand the simplest micellar phase, the BCC, is the least represented, showing up in only 2% of micellar cases.

Table 1. Occurrence (number of reported compounds) of different LC phases in Percec-type dendrons based on benzylether, phenylpropyl ether, biphenyl-4-methyl ether and biphenylpropyl ether of generations 2 and higher (compiled from information in 1).[a,b]

Configuration at root[c]	cubic (A15) ($Pm\bar{3}n$)	tetragonal (σ) ($P4_2/mnm$)	dodecagonal quasicrystal	BCC ($Im\bar{3}m$)
AB3	50 (94%)	0	2 (4%)	1 (2%)
AB2 ortho	42 (91%)	3 (7%)	1 (2%)	0
AB2 meta	7 (37%)	7 (37%)	4 (11%)	1 (3%)
total	99 (**84%**)	10 (**8%**)	7 (**6%**)	2 (**2%**)

[a] Percentages are relative to the total number of occurrences of micellar 3-D phases. [b] Phases occurring in the same compound at different temperatures are also counted. [c] Indicates substitution at the exterior side of the phenyl ring closest to the apex of the dendron: "AB3" = 3,4,5-, "AB2 ortho" = 3,4- and "AB2 meta" = 3,5-substitution.

Table 1 also points to some interesting correlations between molecular architecture and the phase type; e.g. there is large preference for the narrow apex ortho AB2 dendrons to form the $Pm\bar{3}n$ phase in contrast to the wider apex meta AB2 dendrons which show, if anything, a slight preference for the dodecagonal phase and its close approximant the σ-phase. In this communication we concentrate on the BCC phase. At first sight it is indeed surprising that this simple packing is the rarest. In fact, however, there is a group of compounds where the BCC is well represented, i.e. the 3,4,5-tris(alkoxy)benzoate salts of alkali metals or their sulfonate equivalents, as well as some other such AB3 "minidendrons", including those attached to a polymer backbone.[17,35,36,37,38] These can be regarded as 1st generation dendrons; when the alkyl

chains are dodecyl or longer, they all display LC phases of which the BCC occurs at the highest temperatures. All of these salts also form other stable LC phases at lower temperatures. In order to understand this behaviour we first discuss a semiquantitative geometric model that relates molecular shape with the packing mode of the spherical micelles. Since the model predicts that increased branching should stabilize the BCC, we decided to test our model by synthesising new "hyperbranched" alkoxybenzoate salts and test our model's predictions. From the practical viewpoint, if we want to encapsulate guest species into the micelles, thereby inevitably reducing the effective taper angle, we need to start with a wedge as highly tapered as possible in the first place. The second objective is to explore what happens when the terminal chains are not all of the same length, as they have been in most if not all of the previously reported studies.

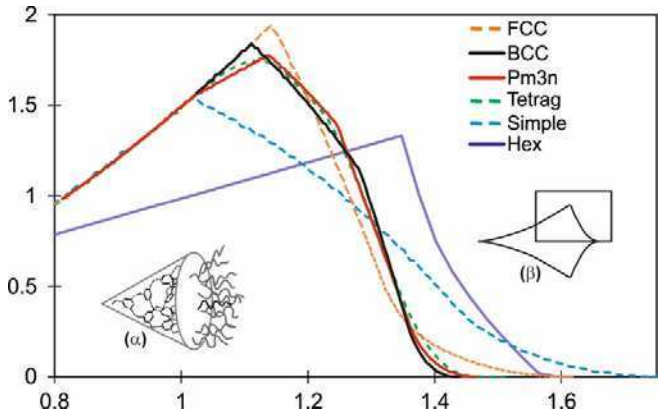

Figure 1 Radial distribution of volume functions *dV/dr* for different micellar phases: face-centred cubic (FCC), BCC, $Pm\bar{3}n$, $P4_2/mnm$ (Tetrag) and simple cubic, as well as for the hexagonal columnar phase (Hex, Col_h). The curves have been normalized to the same total volume of a micelle (disk in the case of Col_h). Abscissa scale is in arbitrary units. For explanation of insets see text (*cf* refs. 32 and 39).

In order to explain why spherical supramolecular dendrimers pack on different lattices, the average radial distribution functions of volume *dV*/*dr* have been calculated for different 3-D lattices with spherical motifs.[32, 39] These functions give the ideal shapes of wedge-shaped molecules that would fill the unit cell of a given phase perfectly uniformly. The spheres of radius *r* are allowed to grow simultaneously from their centres. Let $v_i(r)$ be that part of sphere *i* which does not overlap with another sphere. The graphs in Figure 1 show the averaged functions *dV*/*dr*, where $V = (1/N)\sum_{i=1}^{N} v_i$ is the mean volume *v*, and *N* is the number of spheres in the unit cell. Before the spheres impinge on one another, all curves are parabolae, since the surface of a sphere is $A(r) = dv/dr \propto r^2$. But once they clash, the ascent of d*v*/d*r* either slows down ($Pm\bar{3}n$, tetragonal) or starts to drop (BCC, FCC, simple cubic). Eventually *dV/dr* goes to zero when all space is filled. The shape of *dV/dr* beyond the first clash is different for different lattices. In Figure 1 we also show the *dV/dr* curve for the hexagonal columnar (Col_h) phase. Here the cylinders rather than spheres grow from their central axis; thus *dV/dr* is linear with *r* before the cylinders clash.

A way to relate the *dV*/*dr* functions to the molecular shape is to imagine the conical molecule (inset α in Figure 1) rolled out flat into a parabolic (r^2) fan as schematically drawn in inset β in Figure 1. The ideal envelope of the molecular fan for each phase is represented by the corresponding *dV*/*dr*, with *r* = 0 at the acute apex of the molecule. The rectangle in inset β indicates the limited region of *dV*/*dr* shown in the diagram.

The *dV*/*dr* distribution for BCC differs from those for $Pm\bar{3}n$ and *P*4$_2$/*mnm* in that it has a slightly higher peak and shorter tail. This change in molecular envelope is expected to occur at increasing temperatures due to lateral thermal expansion of the flexible chains requiring a higher *dV*/*dr* peak, and longitudinal contraction of the chains requiring a shorter *dV*/*dr* tail. The *dV*/*dr* curves for $Pm\bar{3}n$ and *P*4$_2$/*mnm* phases are similar to each other, and indeed the two phases have often been found to appear interchangeably.

A brief comment on the FCC phase, whose *dV/dr* is identical to that of the other "close packed" structure, the hexagonal close packing (HCP). Neither have yet been reported in thermotropic tapered compounds. The likely reason is the presence of large octahedral in addition to the small tetrahedral interstices. To reach the centres of the former, a long stretched chain is needed - see the long tail of the *dVdr* curve for FCC. One can speculate that to form the FCC or HCP phase the dendron would have to have perhaps one of the chains very long to match the long tail of the *dV/dr*. Possibly it may also need one or two short branches in addition to comply with the high peak of the FCC curve.

The divergence of the wedge-shaped molecule can be approximated in general by *dV/dr* = kr^p. A rough guide to phase type that such wedge-shaped molecules would form is given as follows.[24] $p \approx 0$: smectic; $0 < p < 1$: bicontinuous cubic; $p \approx 1$: columnar; $p \approx 2$: micellar (cubic or other symmetries). Figure 1 suggests that, as a crude approximation, the value of *p* also plays a part in determining which of the micellar phases is likely to be adopted by the compound, a higher *p* favouring the BCC and a lower *p* favouring the $Pm\bar{3}n$ phase.

Here we explore the high end of *p* and try to make the wedge more "exponential", i.e. make its width increase more steeply at larger *r*. Sodium salts **12^{2}18^{3}Na** and **18^{5}Na** were thus synthesised, each having one of their three alkoxy chains carrying a further three-way branching point based on pentaerythritol. A small branching group is used instead of the usual bulkier phenyl group to keep the wedge narrow near the root (small *r*), and thus increase the divergence *p*. The asymmetric compound **12^{2}18^{3}Na** has the branched chain at the 3-position, and the symmetric compound **18^{5}Na** at the 4-position. Furthermore, while in **18^{5}Na** the five chains are similar in length, in **12^{2}18^{3}Na** they differ in length considerably. These compounds were obtained by Williamson ether synthesis and the tris(alkyloxy)pentaerythritol intermediate was attached to the aromatic group by Mitsunobu reaction. The synthesis is given in Supporting Information (SI). For comparison the AB3 Na salts **12^{3}Na and 18^{3}Na**, with three unbranched $C_{12}H_{25}$ and $C_{18}H_{37}$ chains, respectively, have also been prepared; their synthesis has been described previously.[36] Table 2 gives the phase sequence of the compounds on first heating, as obtained from DSC and X-ray diffraction.

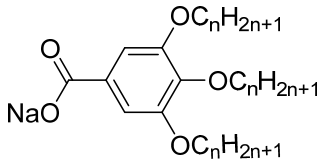

n=12: **12^{3}Na**
n=18: **18^{3}Na**

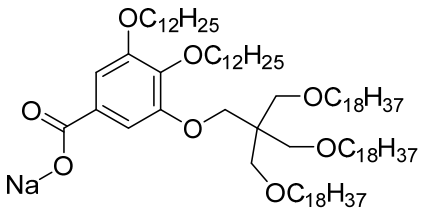

12^{2}18^{3}Na

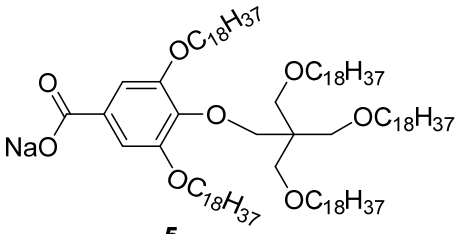

18^{5}Na

Table 2. Phases sequence and transition temperatures of the compounds studied*

Compound	Phases and transition temperatures (°C)
12^3Na	k 70 Col_r 91 Col_h 110 $Pm\bar{3}n$ 220 BCC decomp.
18^3Na	k 84 Col_h 104 BCC decomp
$12^2 18^3$Na	k 39 BCC 200 Iso
18^5Na	k 55 BCC decomp (>270)

*) k = crystal, Col_r = rectangular columnar, Col_h = hexagonal columnar, $Pm\bar{3}n$ and BCC = cubic, iso = isotropic liquid.

Figure 2 shows small-angle X-ray diffraction (SAXD) curves of the mesophases as a function of temperature, recorded during heating of compounds **12^3Na** and **18^5Na**. Equivalent SAXD scans for the other compounds are shown in SI (Figure S2). All compounds show 2D or 3D liquid crystal phases above the crystal melting point. In accordance with previous studies of tris(alkoxy)benzoates,[36] **12^3Na** and **18^3Na** start with the Col_h phase and end up in the BCC (space group $Im\bar{3}m$). In contrast, the hyperbranched compounds **$12^2 18^3$Na** and **18^5Na** melt directly into the BCC phase. Once having reached it, all compounds except **$12^2 18^3$Na** remain in the BCC phase until at least 270°C, where heating runs were interrupted for fear of decomposition. As an exception, **$12^2 18^3$Na** transforms to disordered isotropic liquid at 200°C, as is clear from Figure S2b. There is no detectable associated endotherm, meaning that the transition entropy is extremely low. In all cases the phase sequence is reversed on cooling. The diffraction intensities were used to reconstruct the electron density map of the BCC unit cell (Figure 3b), which clearly shows the spherical maxima at the corners and at the centre of the cell, marking the positions of the aromatic+ionic cores of the micelles. The low density continuum is uniformly filled with the alkyl chains, as indicated by the uniformly green colour in the map.

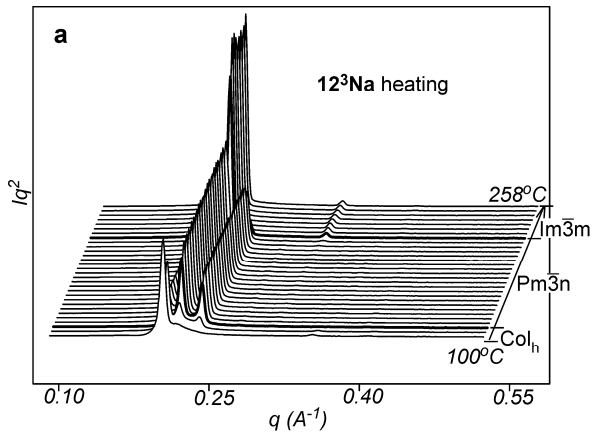

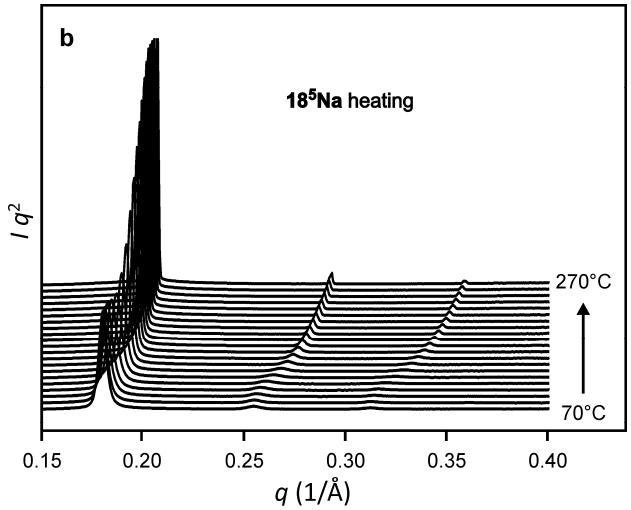

Figure 2. Series of SAXD curves (Lorentz-corrected) recorded during first heating (10 K min^{-1}) of solution-precipitated powder through the mesophase range. (a) **12^{3}Na**; (b) **18^{5}Na**. For clarity the shift between curves is tilted in (a) and vertical in (b). $q = 4\pi\ (\sin\theta)/\lambda$, where θ and λ are half scattering angle and wavelength.

The phase sequence Col_h → $Pm\bar{3}n$ → BCC with increasing *T* for **12^{3}Na** can be understood with reference to Figure 1, by noting the increasingly higher peak and shorter tail of the corresponding *dV/dr* curves. That is, the Col_h curve is suitable for linear wedges, such as found at lower temperatures in **12^{3}Na** and **18^{3}Na**, when their alkyl chains are mainly extended with few *gauche* conformers. At higher *T* and increasing *gauche* content, the chains expand laterally and contract longitudinally. A fan-cone transformation occurs in those two compounds, triggering the columnar – cubic phase transition. If the molecule was confined to a plane, this would be equivalent to a transition from linear to parabolic fan (see inset β in Figure 1), thus requiring the change to a phase structure with a parabolic rather than linear *dV/dr*. As the chain ends of **12^{3}Na** in the $Pm\bar{3}n$ phase continue to expand laterally on further heating, a *dV/dr* function with an even higher peak and shorter tail is required, and hence the $Pm\bar{3}n$ transforms to the BCC. In comparison, however, the longer chains of **18^{3}Na** require such additional lateral space already at lower *T*, which explains why this compound bypasses the $Pm\bar{3}n$ phase altogether.

Turning to the new hyperbranched salts, the fact that these only show the BCC phase is indeed what the *dV/dr* analysis predicts. Already at low *T* their wide aliphatic brushes require the *dV/dr* shape associated with the BCC phase. Their wide end is believed to be made even wider by the well-known preference for alkyl chain ends to adopt *gauche* conformations.[40] Hence these compounds indeed do not show any other LC phase but the BCC.

As temperature is increased, the BCC phase continues. It would appear that no other packing mode offers a better alternative for highly divergent molecules, i.e. a *dV/dr* with a higher peak and shorter tail. This would explain why BCC persists over a range of 200 K or more in most benzoate salts. However this does not prevent the dendrons from continuing to expand laterally and contract longitudinally with increasing *T*. Evidence can be found in the plots of BCC unit cell volume *vs. T* in Figure 3a. The cell volume, and hence the volume of the spheres, *decreases* on heating for all compounds studied, particularly steeply in **18^{3}Na** and **18^{5}Na;** in the latter case the micelle volume nearly halves in the measured *T* range. Our explanation of this remarkable behaviour is in that, as the solid angle Ω of the conical molecule expands, the number of

molecules $\mu = 4\pi/\Omega$, required to complete a sphere, decreases. Furthermore, longitudinal contraction of the chains also means that distant interstices can no longer be reached by the chain ends. Hence in order to fill space the lengthscale of the structure must contract. The thermal effect is equivalent to thermal shrinkage of rubber, an entropically driven phenomenon.[41]

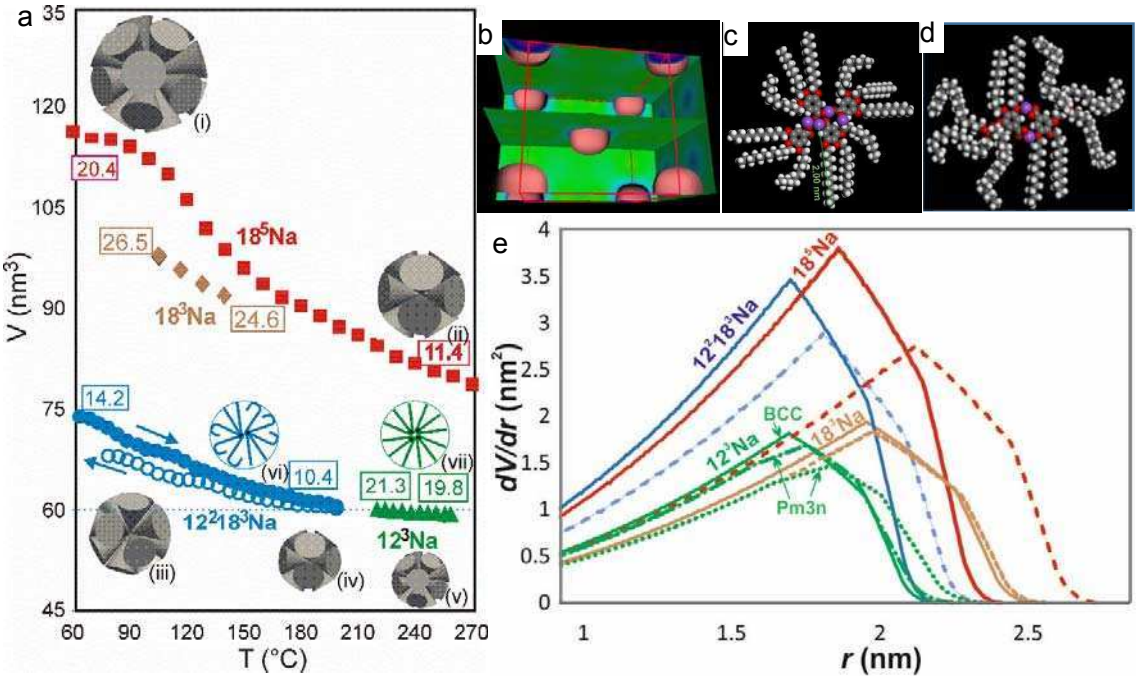

Figure 3. (a) Unit cell volume *vs.* temperature in the BCC phase for the compounds studied. Empty circles refer to a cooling run, full symbols are for heating. Numbers in boxes are numbers of molecules in a sphere (μ) at the low- and high-*T* ends of the associated curves. Insets are described in the text. (b) Electron density map of the BCC phase of compound **$12^2 18^3$Na**. The unit cell is delineated by the red cube. Orange isosurface encloses the spherical regions of high electron density, i. e. the aromatic cores and the ionic part. The colours on the walls and on the z = ½ "shelf" are: green = low (aliphatic), blue-purple = high (aromatic). The structure factor phase angles used are: $\phi_{110} = 0$, $\phi_{200} = \pi$, $\phi_{110} = 0$, $\phi_{211} = 0$. (c,d) CPK models of four molecules of (c) 12^3Na and (d) two molecules of **$12^2 18^3$Na** in a plane representing a likely arrangement in the cross-section of a column (columnar phase) or a sphere (cubic phase). Red = oxygen, purple = sodium. (e) Calculated *dV/dr* curves for the studied compound in the BCC phase and, for 12^3Na, also for the $Pm\bar{3}n$ phase. Here real volume gradients are plotted against real *r* , based on volume and μ data in (a). Dashed and solid curves refer, respectively, to the lowest and highest temperatures of the ranges displayed in (a). Dotted and dot-dash curves are for the $Pm\bar{3}n$ phase of **123Na**.

The thermal shrinkage of the spheres does not imply volume shrinkage of the material. As the compounds are made up mainly of alkyl chains, we have assumed the thermal expansivity to be close to that of liquid n-alkane $C_{16}H_{34}$.[42] Estimating the density at room temperature to be approximately 0.95 g.cm^{-3} based on previous measurements,[36,35] and using the measured cell

volumes and computed densities (see SI, Tables S3 and S4), we calculated μ, the number of molecules per sphere, at the low and high ends of the measured BCC range for all compounds studied – see numbers in boxes in Figure 3a. The spheres made up of the appropriate numbers of cones are schematically shown as insets (i) to (v) in Figure 3a. As *T* increases the surplus dendrons are evidently continuously expelled from the spherical micelles, while at the same time new micelles are formed from the ejected molecules. The largest drop in μ occurs in **18^5Na**, from 20.4 to 11.4. A similarly high rate of dendron ejection is also seen in **18^5Na.** This complex process of disassembly and reassembly of micelles is reversible, as illustrated by the data on unit cell expansion on cooling for **$12^2 18^3$Na** (empty circles in Figure 3a). Some hysteresis is evident at the relatively high applied cooling rate (10 K.min^{-1}). The re-integration of dendrons on cooling is a somewhat slower process than that of their ejection and regrouping on heating.

Thermal contraction of the unit cell has been observed, and ejection of surplus dendrons postulated, also in the case of the columnar phase.[43,35,38] However in that case contraction is only two-dimensional, and one needs to ascertain that a compensating expansion along the column axis does not occur. In fact, when dendrons were covalently attached to a polymer backbone and prevented from leaving the column, the macroscopic fibre has been found to extend longitudinally on heating, in contrast to the usual longitudinal thermal shrinkage of polymer fibres.[43] In free minidendrons, where molecular spacing along the column axis was measured by X-rays, molecular ejection was confirmed as the most likely explanation of lateral shrinkage.[35,38] Nevertheless, there can be no better proof of continuous and reversible thermal disassembly and reassembly than is provided in the case of 3D cubic structures, where thermal shrinkage occurs along all three dimensions, and molecular ejection and reintegration is the only possible mechanism. The presently studied hyperbranched minidendrons provide so far the most compelling examples of this process.

In Figure 3e we show *dV/dr* curves in real scale (nm and nm^2 units) for the actual compounds studied here. As mentioned above, these curves represent the effective wedge shapes of rolled-out molecules (inset β in Figure 1). Figure 3e shows graphically the actual widening and longitudinal contraction of the wedges on heating from the lowest (dashed curves) to the highest *T* (solid curves). These are particularly prominent in **18^5Na** and **18^3Na**. The curves for **12^3Na** also illustrate graphically the equivalent change occurring isothermally upon the transition from $Pm\bar{3}n$ to BCC (*cf.* dot-dash and solid green curves). Note that the end points of the curves in Figure 3e (the length of the wedge) is directly related to the height of the curves in Figure 3a. A further unexpected and counterintuitive finding revealed by Figures 3a,e is that the size of the micelles of **$12^2 18^3$** is exactly the same as that of **12^3Na**, i.e. that the extra pentaerithritol branch with three long C18 chains replacing a single C12 chain made no difference to the length of the molecule and the size of the micelle. The reason can be gathered by comparing the solid blue and green curves in Figure 3e; it shows that all extra material in **$12^2 18^3$Na** had gone into doubling the width of the wedge, rather than extending it. That suggests that the sphere diameter is determined by the shorter chains, the long chains presumably folding back, being highly conformationally disordered or partially interdigitated – see schematics in insets (vi) and (vii) in Figure 3a and molecular models in Figure 3c,d. This illustrates how the molecular conformation adapts to the space filling requirement of the superstructure.

We note that although the *dV/dr* curves give a compelling rationale for many observed features of sequence, structure and size of micellar dendron phases, they should not be considered as the only factors involved. However, it is conspicuous that even if the differences in *dVdr* functions are rather subtle, as e.g. for BCC and $Pm\bar{3}n$ phases, in all compounds where both phases appear, the BCC is invariably the high-*T* phase. Such a clear-cut distinction does not exist between the $Pm\bar{3}n$ and the tetragonal σ-phase, where the *dVdr* functions are very similar indeed.[1,35,36]

CONCLUSIONS

We have prepared the first examples of "hyperbranched minidendrons" of the AB_5 type and shown that the BCC structure provides what seems to be the ultimate mode of thermotropic spherical assembly for highly divergent dendrons. The *dV/dr*-based analysis was shown to be very useful in rationalizing the observed phase behaviour. Thermal shrinkage of supramolecular aggregates via molecular ejection and reassembly has been confirmed beyond doubt, with an unprecedented extent of shrinkage recorded in the **18^5Na** compound. The unexpected behaviour of minidendron **$12^2 18^3$Na** with mixed longer and shorter chains, forming micelles of exactly the same size as **12^3Na**, is attributed to back-folding of the added long chains. The results help improve our general understanding of the complex self-assembly behavour of taper-shaped molecules. We also believe that producing highly divergent dendrons like the hyperbranched ones in this study will allow larger guest molecules to be encapsulated into spherical dendron-based shells.

Acknowledgements. We acknowledge funding from NFSC China (21274132, 21544009), Zhejiang Natural Science Foundation (LY15B020007), Science Foundation of Zhejiang Sci-Tech University (14062016-Y), the joint NSF-EPSRC PIRE program "RENEW" (EP/K034308) and the Leverhulme Trust (RPG-2012-804). G.U. and L. C. are grateful, respectively, for the awards of State Specially Recruited Expert, and High-End Foreign Expert, both from the Government of China. For help with synchrotron SAXS experiments we thank Prof. N. Terrill at I22, Diamond Light Source, UK.

REFERENCES

[1] B. M. Rosen, C. J. Wilson, D. A. Wilson, M. Peterca, M. R. Imam and V. Percec, *Chem. Rev.*, 2009, **109**, 6275-6540.
[2] B. Donnio, S. Buathong, I. Bury and D. Guillon, *Chem. Soc. Rev*. 2007, **36**, 1495–1513.
[3] C. Tschierske, *Angew. Chem. Int. Ed*. 2013, **52**, 8828-8878.
[4] T. Kato, N. Mizoshita and K. Kishimoto, *Angew. Chem., Int. Ed*. 2006, **45**, 38–68.
[5] H.-J. Sun, S. Zhang and V. Percec, *Chem. Soc. Rev.* 2015, **44**, 3900-3923.
[6] F. Würthner, C. Thalacker, S. Diele and C. Tschierske, *Chem. Eur. J.* 2001**, 7**, 2245-2253.
[7] Z. An, J. Yu, B. Domercq, S. C. Jones, S. Barlow, B. Kippelen and S. R. Marder, *J. Mater. Chem.* 2009**, 19**, 6688-6698.
[8] G. Ungar, S. V. Batty, V. Percec, J. Heck and G. Johansson, *Adv. Mater. Opt. Electro*. 1994, **4**, 303–313.
[9] T. Ichikawa, M. Yoshio, A. Hamasaki, T. Mukai, H. Ohno and T. Kato, *J. Am. Chem. Soc.* 2007, **129**, 10662–10663.
[10] M. Peterca, V. Percec, A. E. Dulcey, S. Nummelin, S. Korey, M. Ilies and P. A. Heiney, *J. Am. Chem. Soc.* 2006, **128**, 6713–6720.
[11] C. S. Pecinovsky, E. S. Hatakeyama and D. L. Gin, *Adv. Mater.* 2008, **20**, 174–178.
[12] B. Soberats, M. Yoshio, T. Ichikawa, X. B. Zeng, S. Taguchi, H. Ohno, F. Liu, G. Ungar and T. Kato, *J. Am. Chem. Soc.* 2015, **137***,* 13212-13215*.*
[13] G. Johansson, V. Percec, G. Ungar and D. Abramic, *J. Chem. Soc., Perkin Trans. 1* **1994**, 447-459.
[14] A. Schultz, S. Laschat, A. Saipa, F. Gießelmann, M. Nimtz, J. L. Schulte, A. Baro and B. Miehlich, *Adv. Funct. Mater.* 2004, **14**, 163-168.
[15] V. Percec, M. Glodde, T. K. Bera, Y. Miura, I. Shiyanovskaya, K. D. Singer, V. S. K. Balagurusamy, P. A. Heiney, P. A.; Schnell, I.; Rapp, A.; Spiess, H.-W.; Hudson, S. D.; Duan, H. *Nature* **2002**, *419*, 384-388.

[16] X.-H. Zhang, A. Grant, S. Ellinger, S. A. Odom, D. Sweat, D. B. Tanner, A. G. Rinzler, S. Barlow, J.-L. Bredas, B. Kippelen, S. R. Marder and J. R. Reynolds, *J. Am. Chem. Soc.* 2009, **131**, 2824-2826.
[17] D. J. P. Yeardley, G. Ungar, V. Percec, N. M. Holerca and G. Johansson, *J. Am. Chem. Soc.*, 2000, **122**, 1684-1689.
[18] Y. Tsuda, R. Kuwahara and J.-M. Oh, *Trans. Mater. Res. Soc. Jpn.* **2004**, *29*, 267-271.
[19] A. Grotzky, E. Atamura, J. Adamcik, P. Carrara, P. Stano, F. Mavelli, T. Nauser, R. Mezzenga and A. D. Schluter, *Langmuir* 2013, **29***,* 10831-10840.
[20] V. Percec, A. E. Dulcey, M. Peterca, P. Adelman, R. Samant, V. S. K. Balagurusamy and P. A. Heiney, *J. Am. Chem. Soc.* 2007, **129**, 5992-6002.
[21] B. Donnio, P. Garcia-Vazquez, J.-L. Gallani, D. Guillon and E. Terazzi, E. *Adv. Mater*. 2007, **19**, 3534-3539.
[22] K. Kanie, M. Matsubara, X. B. Zeng, F. Liu, G. Ungar, H. Nakamura and A. Muramatsu, A. *J. Am. Chem. Soc***.**, 2012, **134***,* 808-811.
[23] X. Feng, M. E. Tousley, M. G. Cowan, B. R. Wiesenauer, S. Nejati, Y. Choo, R. D. Noble, M. Elimelech, D. L. Gin and C. O. Osuji, *ACS Nano*, 2014, **8**, 11977–11986.
[24] G. Ungar, F. Liu and X.B. Zeng, "Thermotropic Cubic Liquid Crystal Phases, Other 3D Phases and Quasicrystals" Chap. 7 in **Handbook of Liquid Crystals,** 2nd Ed., Vol. 5, J.W. Goodby, P.J. Collings, T. Kato, C. Tschierske, H.F. Gleeson, P. Raynes eds., VCH_Wiley, Weinheim, 2014, 363-436.
[25] B. P. Hoag and D. L. Gin, *Liq. Cryst.* 2004, **31**, 185-199.
[26] B.-K. Cho, A. Jain, S. M. Gruner and U. Wiesner, *Science*, 2004, **305**, 1598-1601.
[27] P. Ziherl, and R. D. Kamien, *J. Phys. Chem. B*, 2001, **105**, 10147-10158.
[28] Y. Y. Li, S. T. Lin and W. A. Goddard, W. A. *J. Am. Chem. Soc.*, 2004, **126**, 1872-1885.
[29] G. Ungar and X. B. Zeng, *Soft Matter*, 2005, **1**, 95-106.
[30] V. S. K. Balagurusamy, G. Ungar, V. Percec and G. Johansson, *J. Am. Chem. Soc.*, 1997, **119,** 1539-1555.
[31] K. Borisch, S. Diele, P. Göring, H. Müller and C. Tschierske, *Liq. Cryst.*, 1997, **22,** 427-443.
[32] G. Ungar, Y. S. Liu, X. B. Zeng, V. Percec and W. D. Cho, *Science*, 2003, **299**, 1208-1211.
[33] C. H. M. Weber, F. Liu, X. B. Zeng, G. Ungar, N. Mullin, J. K. Hobbs, M. Jahr and M. Lehmann, *Soft Matter*, 2010, **6**, 5390–5396.
[34] X. B. Zeng, Y. S. Liu, G. Ungar, V. Percec , A. E. Dulcey and J. K. Hobbs, *Nature***,** 2004, **428,** 157-160.
[35] G. Ungar, V. Percec, M. N. Holerca, G. Johansson and J. A. Heck, *Chem. Eur. J*., 2000, **6**, 1258-1266.
[36] V. Percec, M. N. Holerca, S. Uchida, W.-D. Cho, G. Ungar, Y. Lee and D. J. P. Yeardley, *Chem. Eur. J.*, 2002, **8**, 1106-1117.
[37] U. Beginn, L. Yan, S. N. Chvalun, M. A. Shcherbina, A. Bakirov and M. Möller, *Liq. Cryst*. 2008, **35**, 1073-1093.
[38] M.-H. Yen, J. Chaiprapa, X. B. Zeng, Y. S. Liu, L. Cseh, G. H. Mehl and G. Ungar, *J. Am. Chem. Soc.* 2016, **138**, 5757–5760.
[39] K. Kanie, M. Matsubara, X. B. Zeng, F. Liu, G. Ungar, H. Nakamura and A. Muramatsu, *J. Am. Chem. Soc.*, 2012, **134**, 808-811.
[40] G. Zerbi, R. Magni, M. Gussoni, K. H. Moritz, A. Bigotto and S. Dirlikov, *J. Chem. Phys.* 1981, **75**, 3175-3194.
[41] We note that some reduction in unit cell volume has also been observed on heating the bicontinuous cubic LC phases – see S. Kutsumizu, H. Mori, M. Fukatami, S. Naito, K. Sakajiri and K. Saito, *Chem. Mater.* 2008, **20**, 3675-3687. However in that case the cause of the contraction is more complex as thermal increase in twist angle between successive molecular layers tends to shorten the distance between network junctions, causing additional unit cell

contraction – see C. Dressel, F. Liu, M. Prehm, X.B. Zeng, G. Ungar and C. Tschierske *Angew. Chem. Int. Ed.,* 2014, **53**, 13115 –13120.
[42] R. A. Orwoll and P. J. Flory, *J. Am. Chem. Soc.* 1967, **89**, 6814-6822.
[43] J.-K. Kwon, S. N. Chvalun, J. Blackwell, V. Percec and J. A. Heck, *Macromolecules* 1995, **28**, 1552-1558.